ULTRA HIGH HEAT FLUX COOLING PROVIDED BY FLOW BOILING IN

MICROSCALE WITH ENHANCEMENTS USING NANOSTRUCTURED SURFACES

by

ALİHAN KAYA

Submitted to the Graduate School of Engineering and Natural Sciences
in partial fulfillment of
the requirements for the degree of
Master of Science

Sabancı University
Spring 2012

ULTRA HIGH HEAT FLUX COOLING PROVIDED BY FLOW BOILING IN

MICROSCALE WITH ENHANCEMENTS USING NANOSTRUCTURED SURFACES

APPROVED BY:

Assoc. Prof. Dr. Ali Koşar ………………………….

(Thesis Supervisor)

Assoc. Prof. Dr. Mahmut Faruk Akşit ………………………….

Asst. Prof. Dr. Güllü Kızıltaş Şendur ………………………….

Asst. Prof. Dr. Gözde Özaydın İnce ………………………….

Asst. Prof. Dr. Burç Mısırlıoğlu ………………………….

DATE OF APPROVAL: 07/06/2012

ULTRA HIGH HEAT FLUX COOLING PROVIDED BY FLOW BOILING IN

MICROSCALE WITH ENHANCEMENTS USING NANOSTRUCTURED SURFACES

Alihan KAYA

Mechatronics Engineering, MSc Thesis, 2012

Thesis Supervisor: Assoc. Prof. Dr. Ali KOŞAR

Keywords: Ultra high mass flux flow boiling in microchannels, Subcooled flow boiling, Boiling instabilities in microchannels, Flow boiling CHF enhancement via surface modifications, Nanostructure coating on microtube walls

ABSTRACT

Due to their heat transfer efficiency and compact implementation methods, the use of flow boiling via plain and modified microchannels for cooling solutions gained a significant importance in the last decade. The increasing need for more efficient cooling solutions in various fields of micro scale cooling such as aerospace, microreactors, automotive industry, micropropulsion, fuel cells, drug delivery systems, biological and chemical applications is motivating researchers to investigate the physics behind the micro scale flow boiling phenomena.

The proposed study aims to make a contribution to the literature in the related field by filling the gap of scientific knowledge about the microchannel flow boiling heat transfer capabilities at ultra high mass fluxes, under unstable boiling conditions and with microchannels having inner wall surface enhancements via nanostructure coating. The present thesis study and results of related experiments are divided into three main parts: ultra high mass flux flow boiling experiments, the effect of inlet restrictions and tube size on premature critical heat flux in microchannels and flow boiling heat transfer enhancement via coating polyhydroxyethylmethacrylate (pHEMA) on inner microtube walls.

In the first part, microchannels having ~250 μm and ~500 μm hydraulic diameters were tested at various ultra high mass fluxes values and different heated length for forcing the conventional heat removal limits of flow boiling via microchannels. De-ionized water was used as working fluid and test section was heated with Joule heating. Wall temperatures for each case were recorded and exit qualities were calculated. The resulting CHF boiling curve demonstrates cooling rates (>30000W/cm^2) that were never achieved by flow boiling in microchannels could be obtained.

In the second part of the present study, useful information about premature CHF phenomena was provided. The study offers a parametric comparative investigation. Experimental data are obtained from microtubes having 250~μm and 685~ μm inner diameters, which were tested at low mass fluxes (78.9-276.3 kg/m^{2}s) to reveal potential boiling instability mechanisms. Moreover, inlet restrictions were introduced to the system for observing their effect in mitigating unstable boiling conditions and extending the boiling curve. De-ionized water was used as a coolant, while microtubes having 5,65 cm heated length were heated by Joule heating. Furthermore, Fast Fourier Transform (FFT) of the deduced data is performed for revealing the frequency correlations of the every obtained temperature and pressure oscillations before and just before the premature dryout condition. The results show the inlet restrictions have a significant effect on reducing the unstable boiling fluctuations and the proposed FFT method was proved to be a useful tool to detect premature dryout before it occurs.

In the third part, flow boiling heat transfer experiments were conducted on microtubes (inner diameter of ~ 250 μm, ~500 μm and ~1 mm) with a constant heated length 2 cm and with enhanced inner surfaces having deposited polyhydroxyethylmethacrylate (pHEMA), which extends the boiling curve, increases the heat transfer surface area, and provides additional nucleation sites. De-ionized water was utilized as the working fluid and test section was heated by Joule heating in this study. Nanostructures on the microtube walls were coated through initiated chemical vapor deposition (iCVD) technique. A significant extension in CHF boiling curve and increase in heat transfer were observed with nanostructure-enhanced surfaces compared to the plain surface counterparts for two relatively high mass velocities, namely, 10000 kg/m^{2}s and 13000 kg/m^{2}s.

MİKRO BOYUTLARDAKİ YÜZEYLER ÜZERİNE NANO-YAPI KAPLAMALARI İLE ÇOK YÜKSEK ISI AKISINDAKİ AKIŞ KAYNAMASININ GELİŞTİRİLMESİ

Alihan KAYA

Mekatronik Mühendisliği, Yüksek Lisans Tezi, 2012

Tez Danışmanı: Doç. Dr. Ali KOŞAR

Anahtar Kelimeler: Mikrokanallarda çok yüksek kütle akısında akış kaynamaları, Aşırı soğutulmuş akış kaynamaları, mikrokanallardaki kaynama kararsızlıkları, Yüzey modifikasyonlarıyla akış kaynaması Kritik Isı Akısı geliştirilmesi, Mikro tüp duvarlarına nano-yapı kaplanması

ÖZET

Düz ve modifiye edilmiş mikro kanallarda akış kaynaması yoluyla soğutma yöntemi yüksek verimli ısı transfer kapasitesi ve kompakt uygulanma metodları sayesinde son yıllarda büyük ölçüde önem kazanmıştır. Uzay mühendisliği, mikro reaktörler, otomotiv endüstrisi, mikro yürütme, yakıt hücreleri, ilaç aktarım sistemleri, biyolojik ve kimyasal uygulamalarda gittikçe artan mikro boyutta daha verimli soğutma ihtiyacı araştırmacıları mikro boyutlarda akış kaynaması yoluyla soğutmayı ve ardında yatan fiziksel faktörleri anlamaya motive etmektedir.

İşbu çalışma, mikro kanallarda çok yüksek kütle akılarında akış kaynaması yoluyla ısı transferi kapasiteleri, kararsız kaynama durumları ve kanal içi nano-yapı kaplamalı yüzey modifikasyonları ile ilgili literatürdeki bilgi boşluğuna katkı sağlamak amacı taşımaktadır. Bu tez ve ilgili deney sonuçları üç ana başlık altında toplanmaktadır: Çok yüksek kütle akılarındaki akış kaynaması deneyleri, tüp girişi kısıtlamaları ve tüp boyutunun mikro kanallardaki kaynama kararsızlıkları üzerindeki etkileri ve iç yüzeyleri polyhydroxyethylmethacrylate (pHEMA) ile kaplı mikro kanallarda akış kaynaması ısı transferi geliştirilmesine yönelik deneyler.

İlk kısım ~250 mikron ve ~500 mikron hidrolik çaplı mikro tüplerde farklı çok yüksek kütle akısı değerlerinde ve farklı ısıtılan uzunluklarda, mikro kanallarda akış kaynaması

yöntemiyle ısı giderme yönteminin bilinen sınırlarını zorlamak amacıyla yapılan deney sonuçlarını içermektedir. Soğutma sıvısı olarak de-iyonize su kullanılmış ve test kısmı Joule ısıtmasıyla ısıtılmıştır. Her deney koşulu için mikrotüp duvarlarındaki sıcaklıklar ölçülmüş ve çıkış kaliteleri hesaplanmıştır. Elde edilen Kritik Isı Akısı grafiği mikro kanallarda akış kaynaması yöntemiyle daha önce ulaşılmamış ısı transferi değerlerine ulaşıldığının göstergesidir.

İkinci kısımda mikrotüplerdeki kaynama kararsızlığı ile ilgili önemli bilgiler sunulmuştur. Çalışma, farklı deney koşullarının parametrik olarak karşılaştırmaktadır. Deneysel sonuçlar, potansiyel kaynama kararsızlığı mekanizmalarını ortaya çıkarmak amacıyla düşük kütle akılarında (78,9 – 276,3 kg/m^{2}s) ~250 mikron ve ~685 mikron hidrolik çaplı tüplerden elde edilmiştir. Ek olarak, tüp girişine konumlandırılan giriş kısıtlayıcılarının kararsız kaynama durumunun azaltılması ve kaynama grafiğinin genişletilmesi üzerindeki etkileri incelenmiştir. Soğutma sıvısı olarak de-iyonize su kullanılmış ve test kısmı Joule ısıtmasıyla ısıtılmıştır. Ayrıca prematüre kuruma durumundan hemen önce ve önce elde edilen sıcaklık ve basınç dalgalanmalarının frekans ilişkilerini ortaya çıkarmak amacıyla Hızlı Fourier Transformu (FFT) yöntemi ile işlenmiştir. Sonuçlar giriş kısıtlayıcılarının kararsız kaynama durumunu azaltmada önemli bir etkiye sahip olduğunu ve FFT yönteminin prematüre kuruma durumunu öngörmek için önemli bir araç olabileceğini kanıtlar niteliktedir.

Üçüncü kısımda ise değişik çaplardaki mikro kanalların (~250 mikron, ~500 mikron ve 1mm) iç yüzeyleri Kritik Isı Akısı grafiğini geliştirmesi, ısı transfer yüzey alanını artırması ve ek baloncuk oluşumu noktaları teşkil etmesi öngörülen polyhydroxyethylmethacrylate (pHEMA) ile kaplanmıştır. Soğutma sıvısı olarak de-iyonize su kullanılmış ve test kısmı Joule ısıtmasıyla ısıtılmıştır. Tüp yüzeyindeki nano-yapılar Başlatılmış Kimyasal Buhar Biriktirme (iCVD) tekniğiyle kaplanmıştır. 10000 kg/m^{2}s ve 13000 kg/m^{2}s kütle akılarında yapılan deneyler sonucunda düz mik ro kanallardan elde edilen sonuçlara nazaran kaplamalı yüzeye sahip mikro kanallardaki Kritik Isı Akısı grafiğinde önemli bir artış gözlenmiştir.

ACKNOWLEDGEMENTS

I would like to thank my thesis supervisor Dr. Ali KOŞAR for his endless support and guidance throughout my study. His willingness to provide 7/24 help in both academic and life issues gave me the biggest motivation to study at his laboratory. I owe him very much and I hope that I've been a sufficient grad student during my time in Sabanci University.

I send my sincere thanks to my ex-colleague Mehmed Rafet Özdemir, from whom I have learned a lot and taken the flag of flow boiling in Sabanci University after him.

I would like to thank Dr. Gözde Özaydın-İnce and her motivated research team, and Dr. Mehmet Keskinöz for their utmost contributions in the projects existing in this study.

I am very thankful to my thesis committee members Dr. Mahmut Akşit, Dr. Güllü Kızıltaş Şendur, Dr. Gözde Özaydın-İnce and Dr. Burç Mısırlıoğlu for giving their precious time for evaluating my MSc thesis.

I also would like to thank to my lab colleagues for their limitless friendship and support. I'd like to thank my colleague Ebru Demir especially for her mother-like support during my overtime thesis writing days, my homie Barış Yılmaz Gündüz for always being on my side, the SUNUM security staff for being my friends in the lonely laboratory nights and my family for the constant psychological support that they provided.

I'd like to present my special thanks to the inventors of Red Bull Energy Drink and Tupac Shakur (R.I.P.) for his lyrics that gave me courage all the time.

TABLE OF CONTENTS

LIST OF TABLES

LIST OF FIGURES

LIST OF SYMBOLS

Latin

A_c	Cross Sectional Area
c_p	Specific heat at constant pressure
d_i	Inner channel diameter
G	Mass Flux
h_{FG}	Latent heat of vaporization
h_{tp}	Two-phase heat transfer coefficient
L_h	Heated Length
$\dot{m}$	Flow rate
MAE	Mean Absolute Error
P	Electrical Power, Pressure
q''_w	Heat flux
$\dot{Q}_{loss}$	Heat loss
r	Experimental value for using in uncertainty
Re	Reynold's number
T_i	Inlet fluid temperature
T_{sat}	Saturation temperature
T_w	Wall temperature
U_r	Result of uncertainty
U_{x_1}	Uncertainty at variable X_1

x_{local} Local mass quality

Greek

μ   Viscosity

Subscripts

i   Inner

e   exit

CHF Value for CHF condition

CHAPTER 1

INTRODUCTION

1.1 General Overwiev of Microchannels

Microchannel is a term used for the channels having hydraulic diameter lower than milimeter scale. Their compactness, high heat transfer capabilities, ease of implementation in various industrial applications, reduced size and weight, less usage requirement of refrigerant material that might be harmful for the environment are the factors that makes microchannel phenomenon an interesting research topic. As the technology goes smaller to the micro and nanosize, the emerged problems usually have to be solved in those scales. The growing MEMS (Micro Electromechanical Systems) industry necessitates microscale problem solving applications. Also the improving speed and reducing size of electronic devices necessitate a proper treatment at small scales.

One of the biggest problems that microscale devices face is the increasing need for cooling. Since every year systems with more heat transfer capability is needed, there is a large palette of research in the field of microscale heat exchangers. There are several examplary problem solving approaches that can be listed as: surfaces having micro pin fins [1], pool boiling applications [2] , flow boiling applications in microtubes [3]. There challanges of heat removal in microscale are pressure drops [4], manufacturing complexity [5], flow instabilities [6], Critical Heat Flux (CHF) conditions that may cause system failure [7].
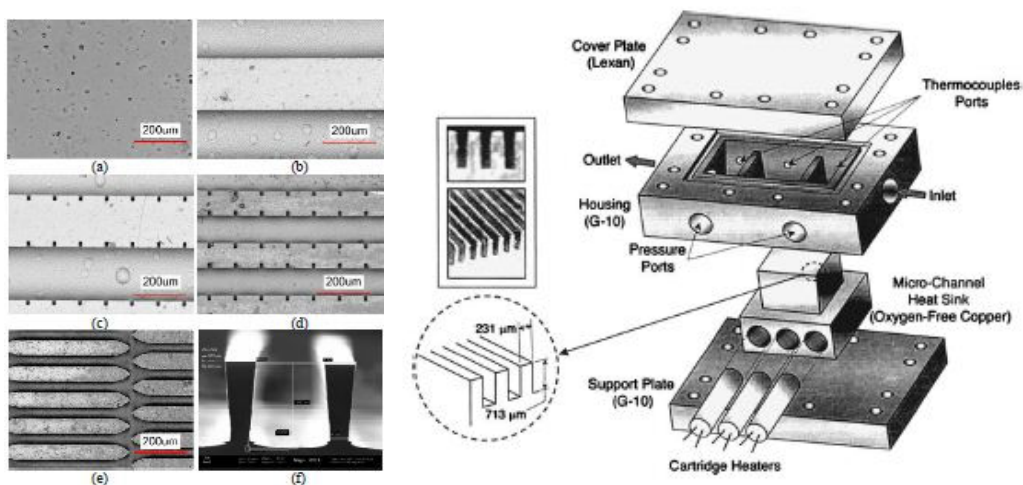
Figure 1-1: Microchannels having various shapes (left) [8] and an examplary flow boiling experiment setup (right) [9]

1.2 Applications of Microchannels

As mentioned before, Over the last decade an astonishing progress in MEMS technology has been witnessed with paramount significance of micro structured devices. From the aspect of microchannel heat exchangers, there are an increasing number of studies in the literature about flow boiling in small channels. As a result of this interest the demand for micro scale cooling devices has been proportionally increased and two-phase flow boiling systems are becoming more important because of their highly effective heat transfer capabilities. They are also practical in numerous microscale applications in addition to electronics cooling such as microchips in microreactors [10], fuel cells [11], drug delivery [12], micropropulsion [13], wireless power transmission [14], thermal actuation [15], medical surgery [16], evaporator applications for air-conditioning [17], micropumps [18] and various MEMS devices [19].

1.3 Objectives and Major Challanges of This Work

The proposed study aims to make a contribution to the literature in the related field by filling the gap of scientific knowledge about the microchannel flow boiling heat transfer capabilities at ultra high mass fluxes, under unstable boiling and premature CHF conditions and with microchannels having inner wall surface enhancements via nanostructure coating. The present thesis study and results of related experiments are divided into three main parts: ultra high mass flux flow boiling experiments, the effect of inlet restrictions and tube size on premature CHF in microchannels and flow boiling heat transfer enhancement via coating polyhydroxyethylmethacrylate (pHEMA) on inner microtube walls.

In the first part, microchannels having ~250 μm and ~500 μm hydraulic diameters were tested at various ultra high mass fluxes values and different heated length for forcing the conventional heat removal limits of flow boiling via microchannels. De-ionized water was used as working fluid and test section was heated with Joule heating. Wall temperatures for each case were recorded and exit qualities were calculated. The resulting CHF boiling curve demonstrates heat transfer values that were never achieved by flow boiling in microchannels.

In the second part of the present study, useful information about microtube premature CHF phenomena was provided. The study offers a parametric comparative investigation. Experimental data are obtained from microtubes having 250~μm and 685~ μm inner diameters, which were tested at low mass fluxes (78.9-276.3 kg/m^{2}s) to reveal potential boiling instability and premature CHF mechanisms. Moreover, inlet restrictions were introduced to the system for observing their effect in mitigating unstable boiling conditions and extending the boiling curve. De-ionized water was used as a coolant, while microtubes were heated by Joule heating. Furthermore, Fast Fourier Transform (FFT) of the deduced data is performed for revealing the frequency correlations of the every obtained temperature and pressure oscillations before and just before the premature dryout condition. The results show the inlet restrictions have a significant effect on reducing the unstable boiling fluctuations and the proposed FFT method was proved to be a useful tool todetect premature dryout before it occurs.

In the third part, flow boiling heat transfer experiments were conducted on microtubes (inner diameter of ~ 250 μm, ~500 μm and ~1 mm) with enhanced inner surfaces having deposited polyhydroxyethylmethacrylate (pHEMA), which extends the Critical Heat Flux (CHF) boiling curve, increases the heat transfer surface area, provides additional nucleation sites. De-ionized water was utilized as the working fluid and test section was heated by Joule heating in this study. Nanostructures on the microtube walls were coated through initiated chemical vapor deposition (iCVD) technique. A significant extension in CHF boiling curve and increase in heat transfer were observed with nanostructure-enhanced surfaces compared to the plain surface counterparts for two relatively high mass velocities, namely 2500 kg/m^{2}s and 3800 kg/m^{2}s.

For having a proper experimental enviroment, a research plan was condcuted:

- The tube fittings and gas valves were installed in a way that even least amount of leakage is prevented, by means of teflon tapes and hardly screwed fittings.
- The microtubes were installed using proper glands for their varying sizes and placed in the setup carefully
- Different pressure sensors, flow meters, thermometers, and Data Acquisition Systems were used specifically for each different experiment condition according to their specifications that was provided by the manufacturer.

- A user interface program was established for each different experiments.
- High power supplier devices were covered carefully for succefully delivering the desired power imput.
- The acquired data were recorded via computer.
- Data reductions were made for premature CHF experiments and the results were discussed
- Data reductions were made for ultra high mass flux flow boiling experiments and the results were discussed
- Data reductions were made for flow boiling experiments in nanostructured microchannels and the results were discussed.

1.3.1 Literature Survey of the Flow Boiling Instability Part

Large palette of microchannel applications is increasingly motivating the researchers towards understanding physics behind microchannel flow boiling. However, working in such small scales comes with potential flow boiling instability problems particularly observed at low flow rates and pressures [20]. Flow boiling instabilities significantly affect the performance of micro fluidic systems and might lead to premature critical heat flux (CHF) [21, 22]. Comprehensive knowledge about critical heat flux is imperative for the extensive use of microchannels in futuristic applications.

Premature critical heat flux in microtubes is regarded as a consequence of upstream compressible volume instability or excursive instability [23]. In the studies reporting two-phase flow instabilities in single channels [24-26], wall temperature and pressure fluctuations were carefully recorded. Kennedy et al. [27] determined the onset of the instability by using pressure drop signals. Several authors also evidenced instabilities in single and parallel micro-channels [27-31]. Kandlikar [29] noted large amplitude fluctuations in multi-channel evaporators. Flow pattern observations revealed a flow reversal in some channels with expanding bubbles pushing the liquid–vapor interface in both upstream and downstream directions [28]. Qu and Mudawar [31] found two types of hydrodynamic instability were identified on a set of parallel channels: 1) severe pressure drop oscillation, which can trigger

the premature critical heat flux, 2) mild parallel channel instability. Consolini and Thome [32] explained such cyclical boiling behavior as liquid filling, bubble nucleation, growth and coalescence of bubbles, vapor expansion of vapor and evaporation of liquid film on walls.

Zhang et al. [33] presented a systematic framework for the transient analysis and active control of microchannel flow oscillations at a system-level view. They developed a lumped oscillator model, which was derived from the momentum balance equation. Their models of predictions from flow oscillations agreed well with the experimental pressure-drop observations across a flow meter and a microchannel heat sink. Chen et al. [34] investigated microchannel heat sink to characterize flow boiling of the perfluprinated dielectric fluid FC-77. The heat sink had 60 parallel microchannels each of 100 μm width and 389 μm depth. Their results showed that in the upstream region, the flow grows from single phase liquid flow at low fluxes to pulsating two-phase flow at high heat fluxes for the duration of flow instability, which starts at a threshold heat flux in the range of 30.5–62.3 W/cm^2 depending on the flow. On the other hand, in the downstream region, they investigated developing flow pattern from bubbly flow, slug flow, elongated bubbles or annular flow, alternating wispy-annular and churn flow, and wall dryout as the highest heat fluxes. They observed that instability occurs under the condition of co-existence of binary states of liquid and two-phase flows in the parallel channels when there is adequate channel flow instability and surface heat flux is less than the heat flux at boiling inception. Moreover, the bulk temperature of liquid did not reach saturation temperature of the channel output.

Bogojevic et al. [35] presented an experimental study of two-phase boiling in a multi-channel silicon heat sink with non-uniform heating using water as the cooling liquid. They integrated thin Ni film sensors, on the backside of the heat sinks in order to gain insight related to temperature fluctuations caused by two-phase flow instabilities under non-uniform heating. They observed that boiling inside microchannels with axially non-uniform heating leads to high temperature non-uniformities in the transverse direction.

Kosar et al. [36] conducted an experimental study about the suppression of boiling flow oscillations in parallel microchannels by inlet restrictors, where water was used as the medium cooling. They deduced a direct relationship between the pressure drop increase imposed by the inlet restrictors and the value onset of unstable boiling. They managed to eradicate the parallel channel and upstream compressible volume instabilities. CHF condition started and triggered at higher heat flux and pressure drops of the system were measured.

For delaying CHF condition and parallel channel instability condition, Kuo and Peles [6] introduced reentrant cavities in microchannels for mitigation. They have observed that the reentrant cavities can mitigate flow boiling instabilities to certain extent. Moreover, the reduced superheat and pressure at the initial stages of bubble nucleation extended the CHF.

Motivated by the abovementioned studies, this study aims to contribute to the literature of boiling instabilities in single microtubes. For this, in order to reveal existing boiling instability mechanisms, experimental data were obtained from single microtube under varying configurations. Experiments were conducted at relatively low mass fluxes (78,9-276,3kg/m^{2}s). De-ionized water was used as working fluid, while the microtube was heated by Joule heating. After the experiments without any inlet restriction, experiments were conducted the same configuration with various inlet restrictions. Temperature and pressure drop fluctuation signals were recorded and processed by using Data Acquisition System and FFT (Fast Fourier Transformation) technique.

1.3.2 Literature Survey of the Ultra High Mass Flux Flow Boiling Part

The performed research in this subject was focused on saturated flow boiling at low mass velocities (G<1000 kg/m^{2}s), where boiling instabilities might impose serious limitations to the extension of micro scale cooling capabilities to higher heat fluxes [37- 38, 39, 40].

Due to the increasing trend in critical heat flux and suppression of boiling instabilities with increasing mass flux flow boiling at high mass fluxes is becoming more and more attractive at higher mass velocities, where subcooled/low quality boiling conditions are expected. As a result, with the shift from low to high flow rates, a transition in critical heat flux mechanism from dryout type critical heat flux to departure from nucleate boiling type critical heat flux is likely to occur [41]. Supplying the working fluid to the tube under subcooled conditions is especially beneficial because of the fluid's ability to extract a significant portion of the supplied wall energy in the form of sensible heat prior to evaporation. This reveals the popularity of subcooled flow boiling in many applications demanding the removal of large heat loads concentrated in small surface areas, such as nuclear cores, radar and directed energy laser and microwave defense electronics [40].

A few experimental studies are present in the literature related to flow boiling and CHF in mini/micro scale at high flow rates and under subcooled flow boiling conditions [40, 42-46]. Recently, Kandlikar [47] developed a predicted method for estimating CHF in mini/microscale flow boiling by considering a large database consisting of CHF data under a broad spectrum of working conditions involving flow boiling at low and high qualities, flow boiling at low and high mass fluxes, flow boiling of different working fluids. His prediction data could successfully predict most of the available CHF data related to mini/micro scale flow boiling. Koşar et al. [48] investigated CHF of water in circular stainless steel microchannels with inner diameters ranging from ~127 μm to ~254 μm at high length over diameter ratios (L_h/d_i>50) over mass velocities ranging from 1,200 kg/m^{2}s to 53,000 kg/m^{2}s. They found that CHF conditions were more dependent on mass velocity and heated length than on exit thermal condition. The results were also compared to six CHF correlations with a mean average error ranging from 22% to 261.8%. They proposed a new supercorrelation to better predict the critical heat flux data under the thermal-hydraulic conditions studied in this investigation as well as in three previous studies.

The literature about subcooled and low quality flow boiling in macroscale is already present and contains some prediction tools [49, 50-51]. However, since scaling laws are not applicable to two-phase flow and flow boiling [50], there is limited information about CHF under subcooled boiling and high flow rate conditions in microscale. This study aims at providing more understanding about critical heat flux phenomenon under these conditions. In this study, short tubes were used to exploit expected CHF enhancement with decreasing length over diameter ratio, to reach high cooling rates (>10000 W/cm^2), and to provide valuable experimental data to literature. Furthermore, with the enhancement in micropumping capabilities, micro scale flow boiling could be performed at higher mass fluxes so that high cooling rates (>10000 W/cm^2) could be attained. New emerging technologies resulting in local heating, where short heating lengths are present, including nano-scale plasmonic applications [52-54], near field radiative energy exchange between objects [55-59], nano thermophotovoltaics [60] could greatly benefit from micro scale boiling heat transfer at high flow rates and short heated lengths. To accomplish this, an intensive experimental work was conducted. De-ionized water was used as working fluid, and the test section was heated for different heated lengths (2-10 mm) by Joule heating method provided by specially prepared thin alligator clips. Mass flux was changed from 20511 kg/m^{2}s to 38111 kg/m^{2}s in microtubes with inner diameters of ~250 μm and ~500 μm, respectively. The effects of mass

flux, length over diameter ratio and diameter on CHF were investigated. Experimental CHF data were compared to the existing subcooled flow/low quality CHF prediction methods.

1.3.3 Literature Survey of the High Mass Flux Flow Boiling on Nanostructre Coated Microchannels Part

The one of the most common phenomena of flow boiling in microtubes is the Critical Heat Flux condition (CHF), where the system cannot bear anymore heat flux. When CHF value is exceeded, undesired consequences may occur, such as abrupt worsening of the heat transfer coefficient between the heating wall and coolant fluid, strong reduction in heat transfer rate, chemical and physical consequences for the wall (fouling, fracture etc.) that could be harmful for the system and its safety [61]. In the literature, there are studies for delaying CHF condition by using micro/nano scale surface enhancements and modifications [62-68].

Khanikar et al. [62] coated rectangular microchannels with carbon nano tubes (CNTs) that were tested for CHF enhancement at high and low mass fluxes. The results showed that the coated CNTs help to enhance the boiling curve. However, the CNTs started to lose their morphology with test repetition, thus resulting in a decrease in CHF enhancement. Sarwar et al. [63] used Al_2O_3 microporous coatings with particle size smaller than 10 μm and coatings thickness of 50 μm in tubes. The increase in CHF was reported to be about 25%. For studying the effects of surface wettability, Phan et al. [64] used silicon oxide (SiOx), titanium (Ti), diamond-like carbon (DLC), and carbon-doped silicon oxide (SiOC) surfaces with static contact angles of 26 deg, 49 deg, 63 deg and 104 deg, respectively, in a single rectangular microchannel having 0,5 mm height, 5 mm width and 180 mm length. The experiments done at 100 kg/m^{2}s showed that more extended boiling curves can be attained at lower contact angles. Morshed et al. [65] performed copper nanowire (CuNWs) coating in the microchannels having 672 μm hydraulic diameters. They grew the nanowires on the bottom surface of the microchannel using electrochemical deposition technique. The two-phase flow experiments at various mass flux and subcooling degrees showed that CuNWs heat transfer rate increased up to ~56%. In the studies of Ahn et al. [66-68] zircaloy-4 CHF performance was investigated in various experimental conditions. The study showed that high wettability of zircaloy-4 micro/nanostructures created by the surface treatments can significantly

enhance CHF during in the annular flow regime as the mass flux increases, which is because of the stability of the liquid film and the liquid replenishment.

As mentioned in the study of Ozdemir et al. [46], as the mass flux increases, the boiling heat transfer mechanism and the CHF mechanism shows a transition from saturated boiling heat transfer to subcooled boiling heat transfer and dryout type critical heat flux to departure from nucleate boiling (DNB) critical heat flux. According to the Kandlikar et al. [69], subcooled boiling involves a locally boiling liquid having a bulk temperature lower than saturation temperature and being exposed to heat flux. The CHF is DNB type and causes a significant increase in the wall temperature. According to the Liquid sublayer dryout model proposed by Celata et al. [70], the nucleated vapor creates a liquid sublayer by forming a vapor blanket at the channel walls around the periphery of the bulk liquid. The CHF takes places after the liquid sublayer evaporates and leads to insulation between the heating surface and the bulk liquid [71], which necessitates a much higher temperature difference for transferring the heat that might lead to undesired system failure [72].
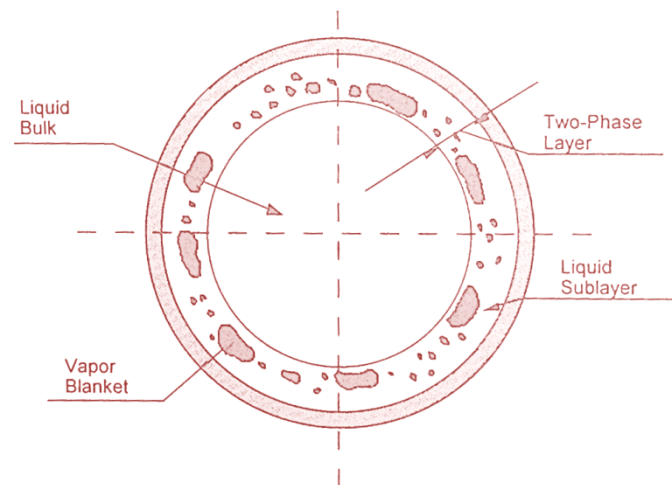
Figure 1-2: Vapor blanket [70]

This study proposes a method for delaying DNB type critical heat flux conditions that are occurring locally on the heated microchannel wall, by means of coating the inner walls of the microchannels having various hydraulic diameters (~250 μm, ~500 μm and ~1 mm) with nanostructures consisting poly-hydroxyethylmethacrylate (pHEMA) which forms superporous hydrogels in aqueous medium. In other words, pHEMA has swelling property in liquid medium and deswelling in dry medium. The acrylic part is the group giving rise to swelling property and, methyl group in pHEMA, on the other hand, determines the strength of the polymer. However pHEMA is mechanically weak in liquid medium. A crosslinker

agent, ethylene glycol dimethacrylate (EGDMA), is used to copolymerize with pHEMA to increase the poor mechanical properties. However, there is an inverse proportion between cross-linker concentration and swelling property, so cross-linker density is held in certain level [73]. Therefore, the swelling property of pHEMA is tested for its capability of forming an extra layer that holds the water within, increases the wettability on the inner tube walls for the working liquid and in this manner delaying the local DNB failure due to CHF conditions. On the other hand, the increased heat transfer area by nanostructures is expected to have a contribution in the heat removal amount. De-ionized water is used as working fluid and the test section (2 cm) is heated by Joule heating. The experiments are done in two relatively high mass flux rates, namely 10000 kg/m^{2}s and 13000 kg/m^{2}s for achieving subcooled boiling conditions. For the performance comparison, the heat transfer rates and wall temperatures at CHF condition for plain and surface enhanced microtubes are measured whereas the exit mass qualities are calculated as well. The steps of performed iCVD methodology are clearly explained in the experimental procedure section.

CHAPTER 2

EXPERIMENTAL SETUP AND PROCEDURE

2.1 Experimental Test Setup

The general overview of the setup used in all experiments is illustrated in the Figure 3. It consists a nitrogen tank for allpying pressure, a microtube test section, water storage tank, flow valves, a presicion valve for restriction, pressure sensors, flow meters, a high level DC power supply and alligator clips connected at the DC poles, a Data Acquisition Unit (DAQ), a computer for the data screening. A detailed illustration of the test section can be seen in the Figure 4. For having proper leakage free fittings teflon tapes were used in every connections.
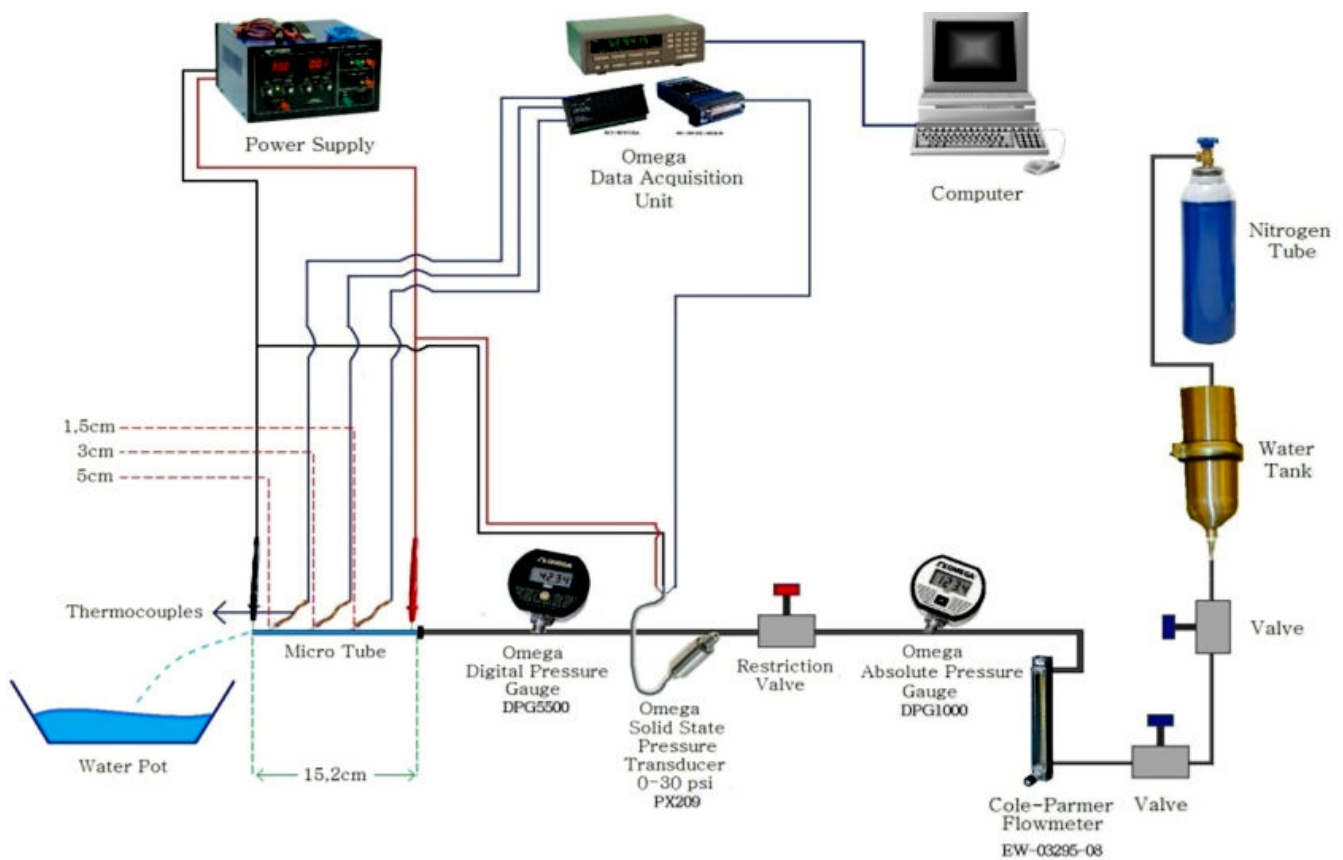
Figure 2-1: The schematic illustration of the experimental test setup
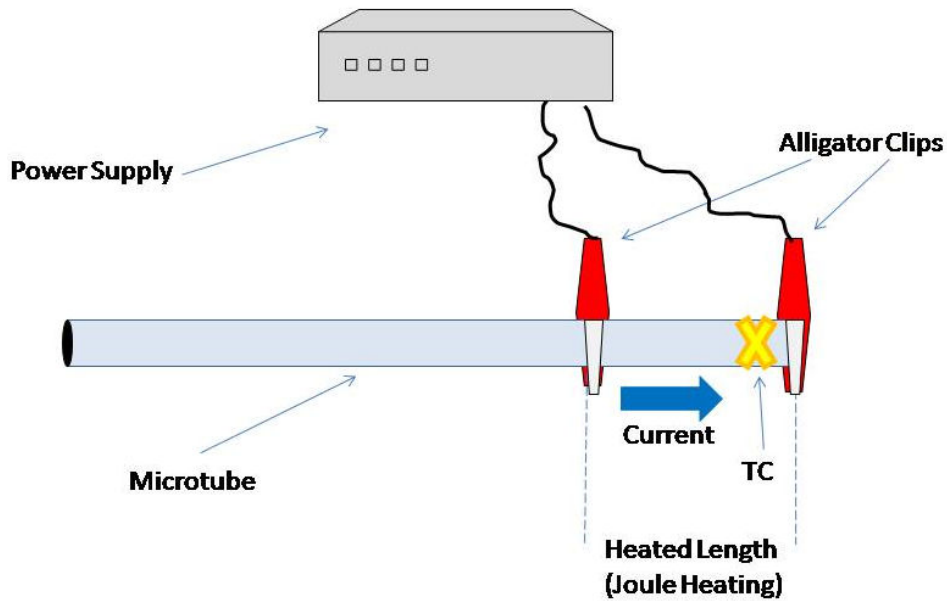
Figure 2-2: A detailed illustration of the test section

The microtube was connected to the experimental loop from one side, whereas the other end was exposed to the atmosphere to ensure atmospheric conditions at the exit. To measure local temperatures, three thin Omega® thermocouple wires (~76 μm thick) were carefully installed to the microtube surface at desired locations using Omega® Bond. Inlet pressures were measured manually via two Omega® pressure transducers with a 0 to 3000 psi gauge pressure range, for achieving measurement even in high fluid velocities. In the second step of the experiments, a restriction valve just before the microtube was inserted. A digital pressure sensor was installed before the test section, which provides the measure pressure and is connected to DAQ (Data Acquisition System). Furthermore, flow rate data was obtained together with the voltage, current, wall/fluid temperatures, and pressures, which were acquired through a LabView® interface with time and were transferred to a spreadsheet file for data reduction.

2.2 Experimental Procedure

During the experiments, the flow rate was fixed at the desired value by adjusting the pressure difference between the inlet and exit. It was made sure that temperatures and pressure values obtained from the Labview® interface did not significantly change with time so that experiments could be performed after steady flow conditions were reached. The power was increased in ~0.3 Ampere increments until the test section loses its uniformity due to overheating, which was considered as CHF condition. The current/voltage, inlet pressures and inlet temperatures were acquired under steady state conditions. This procedure was repeated for different flow rates. The flow chart of the general experimental procedure can be seen in the Figure 5:
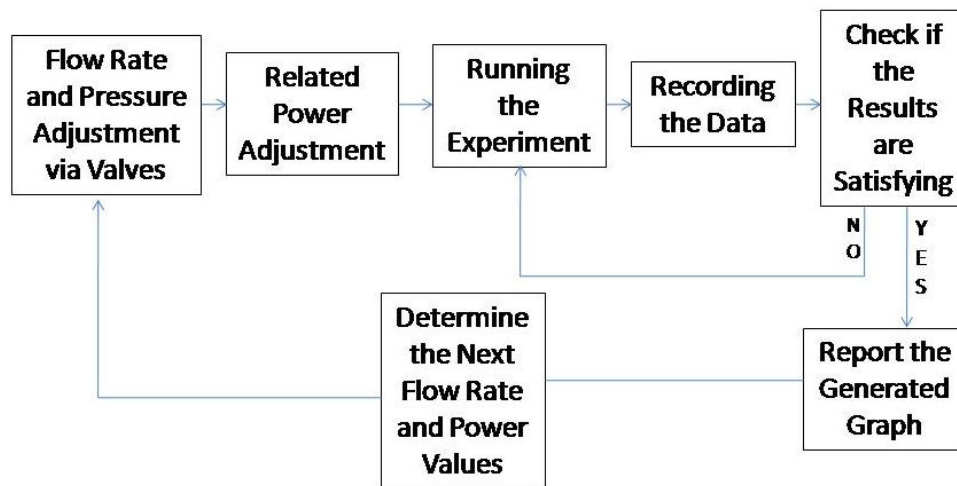
Figure 2-3: General flowchart of the experiments

The estimation of heat loss ($\dot{Q}_{loss}$) was done by applying electrical power to the test section when there is no flow. The temperature difference between the test section and ambient environment was measured. A heat loss curve was deduced with respect to the wall temperature and used for calculation in every experimental condition. For every experiment, De-ionized water was used as working fluid and test section was heated with Joule heating.

For every different part of this study, different experimental conditions were used to attain the data. In the first part of the present study, experimental data were obtained from microtubes having 250~μm and 685~ μm inner diameters and constant 5,65 cm of heated length which were tested at low mass fluxes (78.9 - 276.3 kg/m²s) to reveal potential boiling

instability mechanisms. Moreover, inlet restrictions were introduced to the system for observing their effect in mitigating unstable boiling conditions and extending the boiling curve. In the second part, microchannels having ~250 μm and ~500 μm hydraulic diameters were tested at various ultra high mass fluxes values (20511 kg/m^{2}s to 38111 kg/m^{2}s) and different heated lengths (2 - 10 mm) for forcing the conventional heat removal limits of flow boiling via microchannels. Wall temperatures for each case were recorded and exit qualities were calculated. In the third part, flow boiling heat transfer experiments were conducted on microtubes (inner diameter of ~ 250 μm, ~500 μm and ~1 mm) with enhanced inner surfaces having deposited polyhydroxyethylmethacrylate (pHEMA) and nanostructure-enhanced surfaces compared to the plain surface counterparts for two relatively high mass velocities, namely 10000 kg/m^{2}s and 13000 kg/m^{2}s.

2.3 Deposition Methodology of pHEMA

Substrates with 3-D geometric limitations can be easily deposited by iCVD with great homogeneity and with improved control on the thickness of coatings. Basically iCVD is in the class of hot wire chemical vapor deposition (HWCVD) techniques; and important advantages of iCVD have been realized by the researchers. Working principle of iCVD is consistent with known free radical polymerization reaction mechanism and components of the system are illustrated in Figure 2-4 [26].
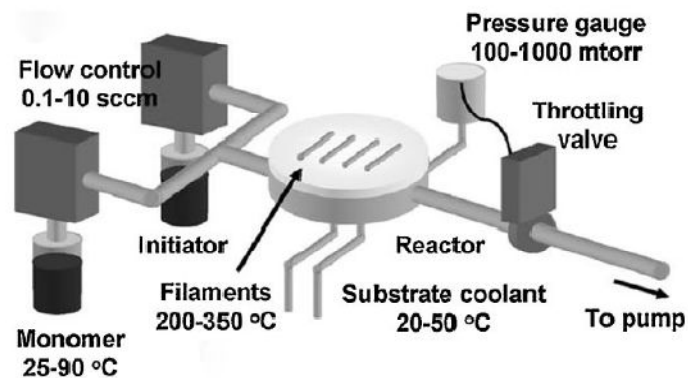
Figure 2-4: Schematic of iCVD system and the components [26]

The polymerization takes place in three steps: initiation, propagation and termination. The process is performed in the vacuum chamber (P @ 10^{-1}-1 Torr) and initiator is fed in the system which is decomposed by heated filaments. Monomer and (if used) cross linker agents are heated to certain temperature in order to obtain vapor pressure of these monomers and cross-linkers. The radicals created by the heated filaments meet the adsorbed monomers on the substrate stage and start the polymerization. The stage is maintained at room temperature, which increases the adsorption rate of gas phase molecules on the substrate. Temperature of filaments and stage can be tuned by different panels and the control over the experimental conditions is improved. Kinetics of iCVD are well studied for various materials, and the kinematic effect of the experimental conditions (i.e. system pressure, filament temperature, stage temperature, feed rates of reactants) can be easily conceived by different researches [89].

Table 2-1: Experimental conditions for iCVD deposition of poly (HEMA-co-EGDMA) into the metal pipes

	Reactant function	Flow rates, F (sccm)	P_m/P_{sat}	Temp (^{0}C)	Total Pressure (Torr)
TBPO	Initiator	1	0,0023	270	
EGDMA	Crosslinker	0,12	0,59		
HEMA	Monomer	0,86	0,326		
Nitrogen	Diluting element	1			
					0,21

2.4 Data Reduction and Uncertainty Analysis

The data obtained from the voltage, current, flow rate, temperature, and pressure measurements were used to obtain two-phase heat transfer coefficients, and local qualities. Reynolds number is expressed as:

$$\text{Re} = \frac{Gd_i}{\mu} \tag{1}$$

where G is mass flux, d_i is channel inner diameter , and μ is viscosity. The mass flux G is given by:

$$G = \frac{\dot{m}}{A_c} \tag{2}$$

where $\dot{m}$ is mass flow rate, and A_c is cross sectional area of the channel. The electrical input power and resistance were calculated using the measured voltage and current values.

The critical heat flux was obtained using the microchannel dimensions and the net power according to:

$$q''_{CHF} = \frac{\left(P - \dot{Q}_{loss}\right)}{\pi d_i L_h} \tag{3}$$

Exit mass quality was deduced based on energy balance:

$$x_{e,CHF} = \frac{q''_{CHF} \pi d_i L_h - \dot{m} c_{p,e}\left(T_{sat,e} - T_i\right)}{\dot{m} h_{FG,e}} \tag{4}$$

where $\dot{m}$ is mass flow rate, c_p is specific heat, T_i is inlet temperature, and h_{FG} is latent heat of vaporization. EES® Software is used to reduce the experimental data to the desired above mentioned parameters in the current study.

The two-phase heat transfer coefficient is calculated as:

$$h_{tp} = \frac{(P - \dot{Q}_{loss})}{\pi d_i L_h (T_{w,i} - T_{sat})} \tag{5}$$

The uncertainties of the measured values in three different parts are given in Table 1-3. They were provided by the manufacturer's specification sheet, whereas the uncertainties were obtained using the propagation of uncertainty method developed by Kline and McClintock [41]. According to this method, if for an experimental result, r, computed from J measured variables $X_{1...J}$, the data reduction equation is:

$$r = r(X_1, X_2, \ldots, X_J) \tag{6}$$

then the corresponding uncertainty in the experimental result is given by:

$$U_r^2 = \left(\frac{\partial r}{\partial X_1}\right)^2 U_{X_1}^2 + \left(\frac{\partial r}{\partial X_2}\right)^2 U_{X_2}^2 + \cdots + \left(\frac{\partial r}{\partial X_J}\right)^2 U_{X_J}^2 \qquad (7)$$

where U_r is the uncertainty in the result, U_{XI} is the uncertainty in the variable X_1, etc. Moreover, the outer diameters were directly measured using a high precision caliber with an uncertainty of ±1 μm. The inner diameter was carefully obtained by relating it to the outer diameter via visualization through computer vision techniques.

Table 2-2: Uncertainties in experimental parameters for the first part

Uncertainty	Error
Flow Rate, ṁ (for each reading)	± 1.0 %
Voltage supplied by power source, V	± 0.1 %
Current supplied by power source, I	± 0.1 %
Temperature, T	± 0.1 ˚C
Electrical power, P	± 0.15 %
Mass flux, G	± 2.7 %
Hydraulic diameter, d_i	± 1 μm
Heated Length, L_h	± 1 μm
Heat Flux, q"	±3.5%

Table 2-3: Uncertainties in experimental parameters for the second part

Uncertainity	Error
Flow Rate, Q (for each reading)	±1,0%
Voltage supplied by power source, V	±0,1%
Current supplied by power source, I	±0,1%
Temperature, T	±0.1˚C
Electrical power, P	±0,15%
Pressure drop, ΔP	±0,25%
Mass flux, G	±2,7%

Table 2-4: Uncertainties in experimental parameters for the third part

Uncertainty	Error
Flow rate, $\dot{m}$ (for each reading)	±1.0%
Hydraulic diameter, d_i	±1 μm
Temperature, T	±0.1ºC
Electrical power, P	±0,15%
Heat flux, q''	±3.5%
Mass Flux, G	±2,7%
Heated Length, L_h	±1 μm
Heat transfer coeff., h_{tp}	± 10.7%

CHAPTER 3

RESULTS AND DISCUSSIONS

3.1 First Part - Flow Boiling Instability

In this section, experimental premature CHF results due boiling instabilities in tubes having 254 μm and 685 μm inner diameters are presented. Temperature fluctuations and pressure fluctuations will be discussed under the different inlet restriction conditions and different mass fluxes. To further characterize the temperature and pressure fluctuations, FFT of these fluctuations were taken and the comcomitant results will be discussed.

3.1.1 Boiling Curves

Boiling curves for every inlet restriction configuration with the increasing mass flux are shown in Figure 6. The attained experimental data demonstrate that the inlet restrictions have significant effect on expanding the boiling curve, by increasing the threshold for premature CHF inception. Moreover, the comparison between the three configurations shows that the heat flux corresponding to premature CHF inception rises exponentially in parallel lines with Koşar et al. [36] as the restriction ratio is increased.

However, it should be noted that the microtubes failed after a slight increase in the heat flux just before the premature CHF condition so that no further temperature and pressure signals could be attained beyond these points. It was found that the change in microtube inner

diameter and the ratio of inlet restriction have a significant effect on delaying premature CHF inception condition. The boiling curve was extended to higher heat fluxes with 4:1 and 8:1 inlet restriction configurations while boiling instabilities appear just after boiling inception for the case without inlet restriction. When the 4:1 inlet restriction was introduced to the system, the attained maximum heat flux rise at four different mass flux values ranging from 78.9 kg/m^{2}s – 276.3 kg/m^{2}s was observed to be 35.8%, 33.1%, %17.1 and 16.4%, respectively, than the results attained from microtubes without inlet restrictions. In the next step, the enhancement in restriction ratio up to 8:1 yielded much better resultsfor the same mass flux values, which were 61.9%, 61.6%, 41.3% and 25.6%, respectively.
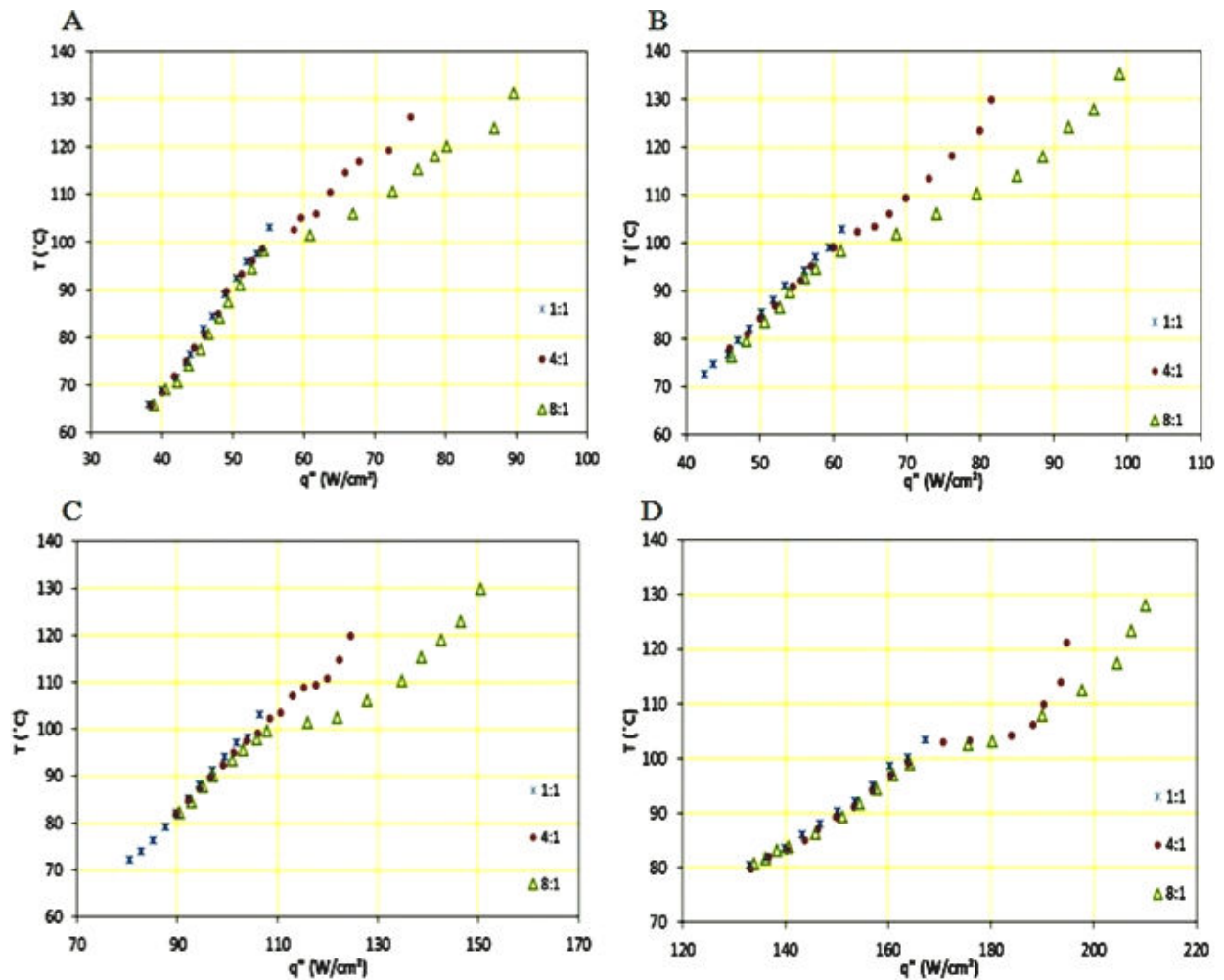
Figure 3-1: Corresponding boiling curves of the 254μmmicrotubes having 1:1, 4:1 and 8:1 inlet restriction ratiosat various mass fluxes A) 78.9 kg/m^{2}s B) 98.7 kg/m^{2}s C) 157.6 kg/m^{2}s and D) 276.3 kg/m^{2}s

On the other hand, the effect of microtube hydraulic diameter can be observed from the Figs. 3-1 & 3-2 as well. With the increasing diameter, CHF improvement seems to be less effective and the inlet restriction configurations have less effect on expanding the CHF boiling value. For each different mass flux value, the amount of curve expansion in the microtube having 685μm inner diameter decreases significantly. In larger scales, the inlet restrictions become relatively less effective and the lesser curve expansion becomes more obvious as the mass flux increases. In the 685μm diameter tube the maximum heat flux for 1:1 restriction ratio decreases down to 40,3% , with 4:1 restriction ratio to 45.6% and with 8:1 restriction ratio to 45.7% of the expansion yielded by 254μm diameter, respectively. This performance difference between varying microtube diameters could be related to more dominant bubble-channel interaction in smaller scales, which contributes to boiling instabilities while bubble-channel interaction is less likely to occur for larger size tubes.
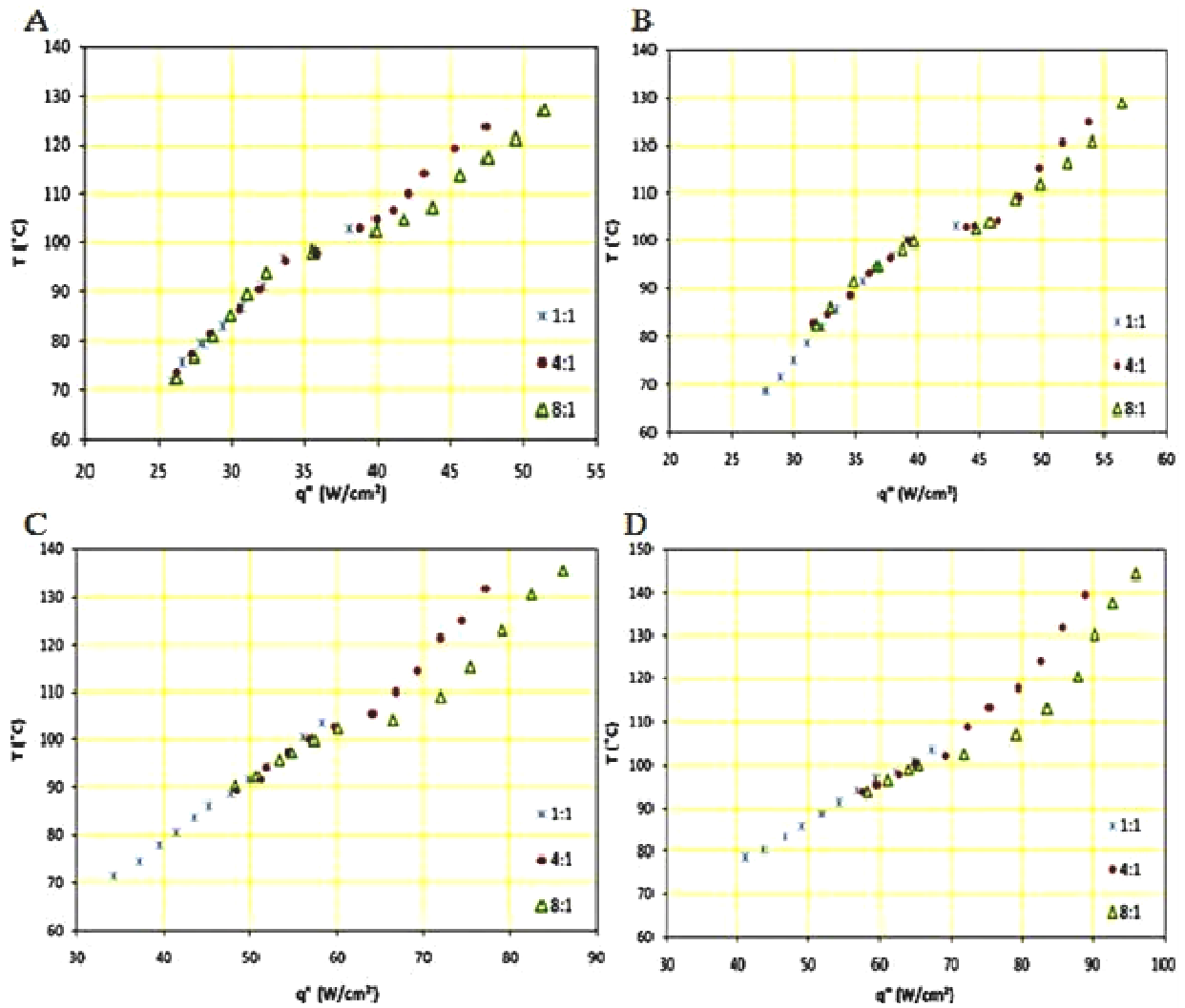
Figure 3-2: Corresponding boiling curves of the 685μm microtubes having 1:1,4:1 and 8:1 inlet restriction ratios at various mass fluxes A) 78,9 kg/m^{2}s B) 98,7 kg/m^{2}s C) 157,6 kg/m^{2}s and D) 276,3 kg/m^{2}s

3.1.2 Wall Temperature and Pressure Fluctuation Results

Temperature fluctuations at different mass and heat fluxes given in Figure 3-3 are recorded just before premature dryout. The premature dryout conditions occur after a gradual increase in power. The effect of inlet restrictions on temperature fluctuations can be observed from Figure 3-3. From the observations on the fluctuation behavior, it was deduced that the

difference between peak to peak points of temperature shows a decreasing tendency as the restriction ratio increases. For four mass flux values ranging from 78.9 kg/m^{2}s to 276.3 kg/m^{2}s, temperature peak to peak differences in 254μm inner diameter tube having 4:1 restriction ratio vary between 91% - 76% of the values corresponding to without inlet restrictions. In the 8:1 inlet restriction ratio case, the same comparison demonstrates an amplitude reduction down to 67% - 40% of the non-restricted case. The same experiments on 685μm inner diameter tube with 4:1 inlet restriction ratio results in a reduction ratio between 98%-78%, whereas 8:1 inlet restriction case yields 75%-51% of the values obtained from microtube with non-restricted inlets. Moreover, the temperature fluctuation amplitudes decrease with increasing mass flux. As MacBain and Bergles [74] stated in their study, the possible reason for this trend is that an increase in mass flux causes an increase in heat transfer coefficient in the convection-dominated regime, where the forced convective heat transfer takes place through liquid film, which mitigates the temperature fluctuation behavior until the inception of boiling instability. In the smaller scale case, the fluctuation periods tend to increase (namely, from approx. 3s to 2s .t G = 78,9 kg/m^{s}s and 15s to 9s at G = 276.3 kg/m^{2}s) by the increasing mass and heat flux, and the periods tend to become longer in the setups without inlet restriction, as can be observed from Figures 3-3-A and 3-3-B. On the other hand, inlet restrictions yielded a significant increase in average fluctuation temperatures, which is probably a result of less unstable boiling features delaying the microchannel dry-out by preserving the liquid thin film on the microtube walls for a longer while.
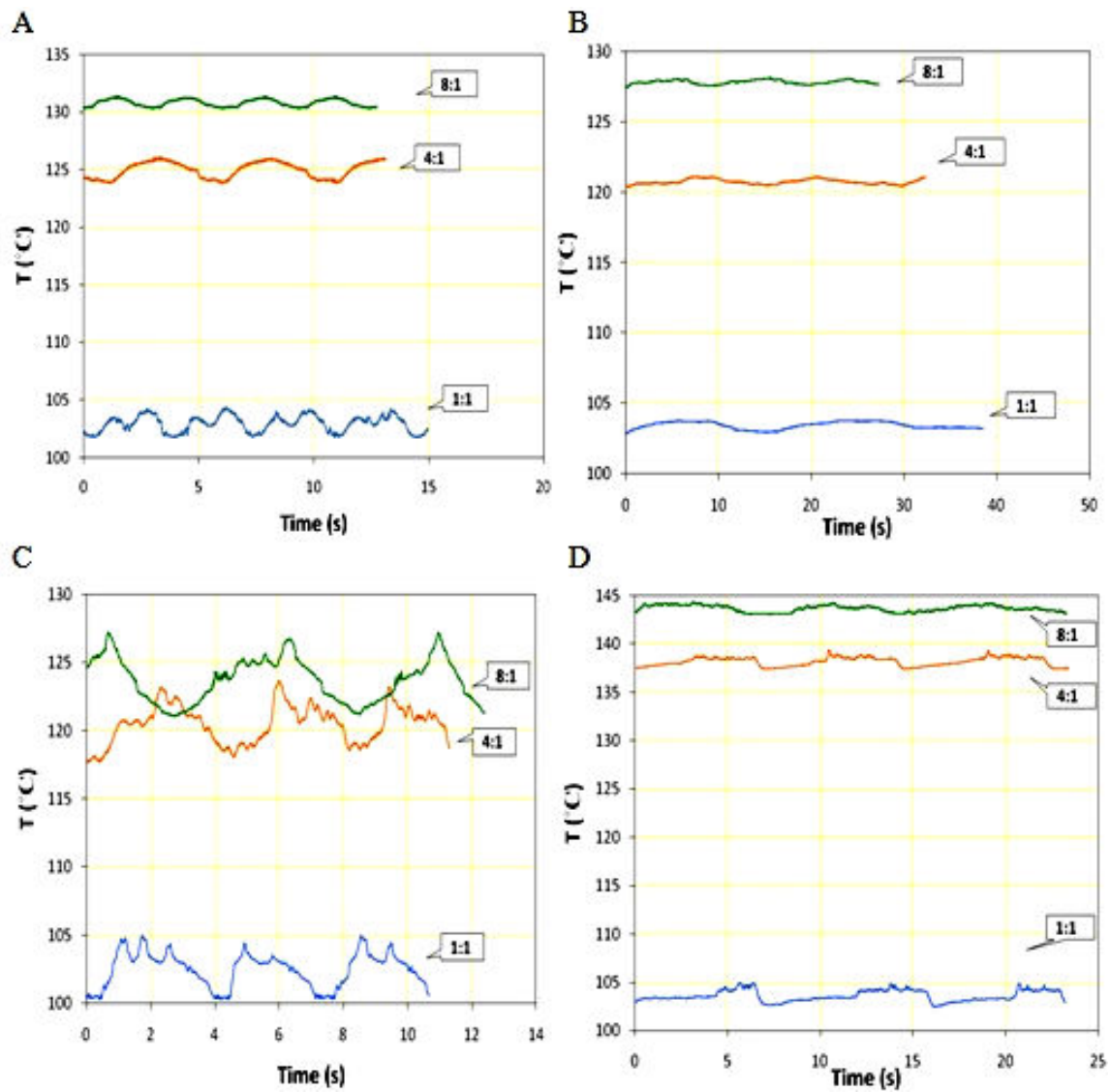
Figure 3-3: Temperature fluctuation profiles of 1:1,4:1 and 8:1 inlet restriction ratios of A) 254 μm microtube at 78.9 kg/m^{2}s mass flux, B) 254μm microtube at 276.3 kg/m^{2}s mass flux, C) 685μm microtube at 78.9 kg/m^{2}s and D) 685 μm microtube at 276.3 kg/m^{2}s mass flux

Furthermore, the temperature fluctuations are shown before the premature dryout in Figure 3-4 for demonstrating the change in fluctuation behavior from stable boiling to unstable boiling. It can be clearly observed that before the premature dryout, the fluctuation amplitudes are much less in comparison to the amplitudes just before the premature dryout, while the fluctuation periods do not significantly change. In the literature [75, 76], the instability mechanism with relatively large periods is considered as type of instability, while the bubbly/slug flow and elongated slug/semi-annular flow is taking place during the two-phase

flow bubble dynamic instabilities. Overall, inlet restrictions causing a restriction for vapor movement to the inlet yielded significantly less instabilities in comparison to the 1:1 ratio test setup in both diameters and for all different mass fluxes.
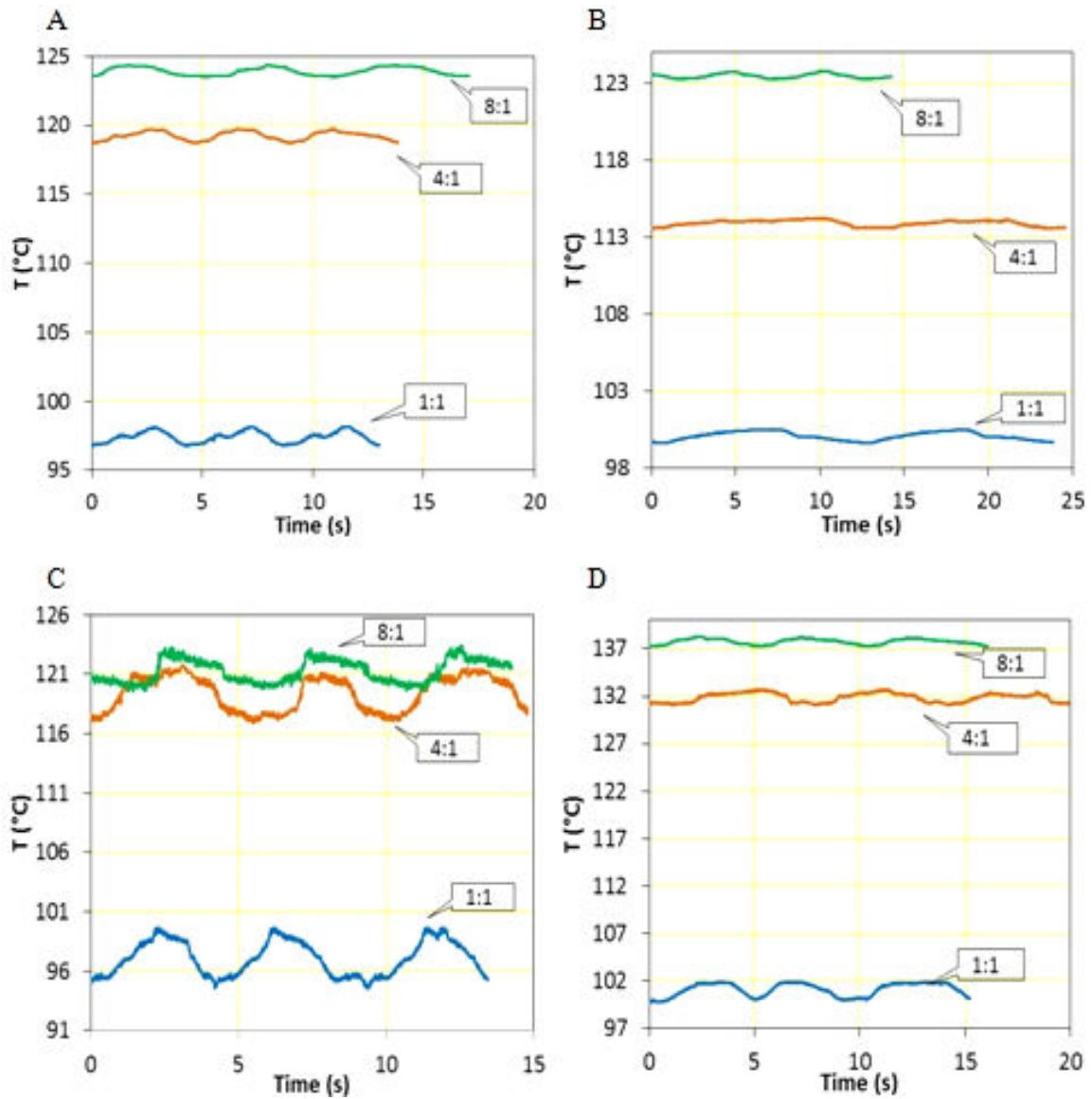
Figure 3-4: Before premature dryout condition temperature fluctuation behaviors of 1:1, 4:1 and 8:1 inlet restriction ratios of A) 254 μm microtube at 78,9 kg/m^{2}s mass flux, B) 254μm microtube at 276,3 kg/m^{2}s mass flux, C) 685μm microtube at 78,9 kg/m^{2}s and D) 685 μm microtube at 276,3 kg/m^{2}s mass flux

The pressure fluctuation obtained from 254 μm microtube can be observed in Fig. 3-4. The inlet restrictions have a significant effect on suppressing the unstable pressure fluctuations during boiling. Similar to the temperature fluctuation profiles, a decreasing tendency in peak to peak pressure differences was observed with increasing restriction ratio. In 254 μm microtube having 4:1 restriction ratio, pressure fluctuation peak to peak amplitudes are reduced down to 93%-88%, and in microtube with 8:1 restriction ratio pressure fluctuation amplitude drops down to 80%-66% of the values deduced from microtube with non-restricted inlet. The fluctuation periods do not show a clear difference with the changing inlet restriction ratio for constant mass flux, which is approximately 5.5 - 7s at G=78.9 kg/m^{2}s and 12.5 - 14s at G=276.3 kg/m^{2}s.
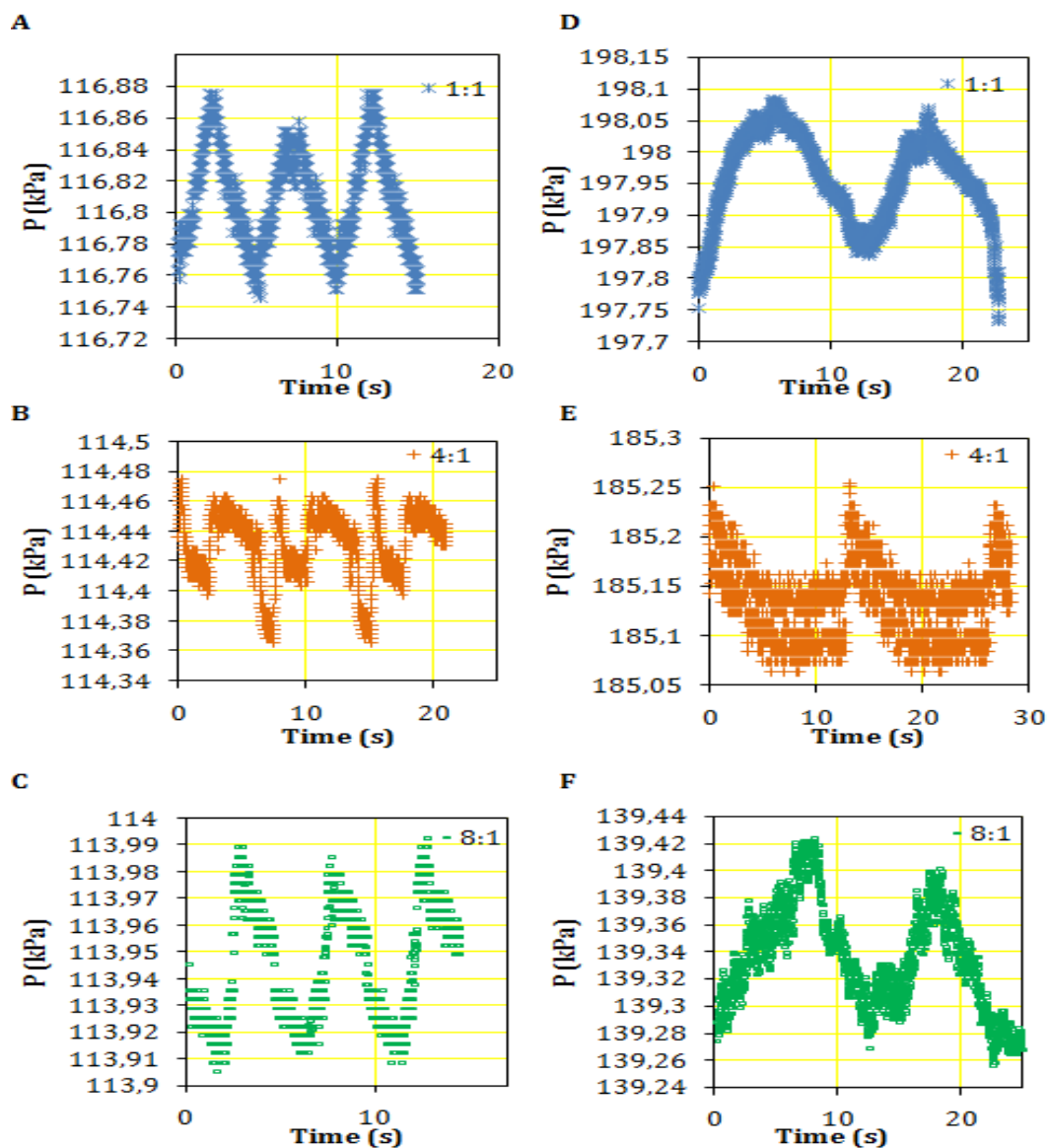
Figure 3-5: Pressure fluctuation profiles for 254 μm microtube at mass fluxes A-C) 78,9 kg/m^{2}s and D-F) 276,3 kg/m^{2}s for every inlet restriction condition

In the case of 685 μm inner diameter microtube, 4:1 restriction yields peak to peak pressure fluctuations of 91% - %82 of the values obtained from non-restricted inlets, whereas 8:1 restriction yields peak to peak pressure fluctuations of 83% - 64% of the values obtained from non-restricted inlet (Fig. 3-6). The fluctuation periods seem to remain unaffected for constant mass flux (approximately 4.5 - 6s at G=78.9 kg/m^{2}s and 5 – 6.5s at G=276.3 kg/m^{2}s) similar to temperature fluctuations.
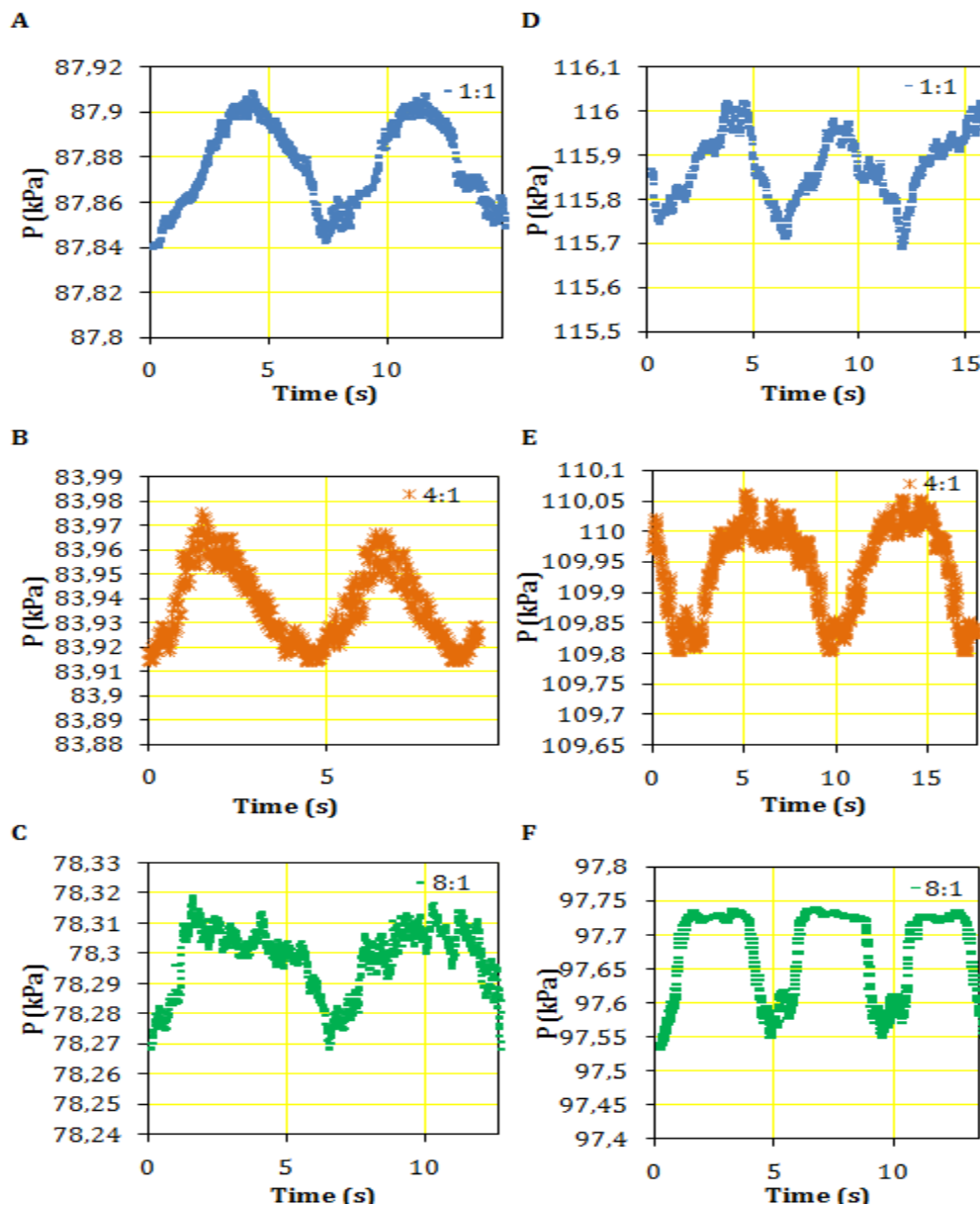
Figure 3-6: Pressure fluctuation profiles of 254 μmmicrotube at 78,9kg/m^{2}s mass flux (A to C) and at 276,3 kg/m^{2}s mass flux (D to F)

On the other hand, similar to the temperature fluctuation profiles, the increasing mass flux leads to lesser peak to peak pressure differences. As Brutin and Tadrist reported a related case in their study [77], this decrease in amplitudes is probably related to the fact that at higher Joule heating and mass flux conditions, namely as the flow demonstrate thinner liquid film-larger vapor core characteristics, the microtube exit vapor quality reaches to 1 with the increasing Reynolds number, which leads to lower vapor pressure fluctuations.

3.1.3 FFT Results

In order to reveal the temperature fluctuations between the cases of before premature CHF and just before premature CHF, some statistical variations of the temperature readings were determined. Let $x(t)$ denote the temperature reading at time t and assume that N temperature measurements were taken in time with a sampling period T_s as:

$$x[n] \equiv x(nT_s) \text{ for } n = 0,...,N-1 \tag{8}$$

where n denotes the time index of the sample taken at $t = nT_s$.

To quantify the change in the temperature signals at the initiation of premature CHF, for different mass flux densities, restriction ratios and diameter sizes, mean value, standard deviation and minimum and the maximum of the signal envelope in time were calculated respectively as:

$$
\begin{aligned}
\bar{x} &= \frac{1}{N}\sum_{n=1}^{N} x[n] \\
\sigma &= \sqrt{\frac{1}{N}\sum_{n=1}^{N}(x[n]-\bar{x})^2} \\
x_{\min} &= \min_{n=0,1,...,N-1} |x[n]| \\
x_{\max} &= \max_{n=0,1,...,N-1} |x[n]|
\end{aligned}
\tag{9}
$$

As can be seen from the Tables 3-1 to 3-4, the statistics $\bar{x}$, x_{min} and x_{max} in Eq. (9) increase whereas σ decreases as the restriction ratio or mass flux increases irrespective from the stability condition. After the inception of premature CHF, these statistics get higher as compared to their values before instability for the same set of experimental parameters.

Table 3-1: Some Features of Temperature Measurements Before Premature Dryout for diameter 254 μm

	Flux 78.9			Flux 276.3		
	1:1	4:1	8:1	1:1	4:1	8:1
Minimum of Time Domain Envelope	96.7391	118.6848	123.5302	99.6246	113.5465	123.2588
Maximum of Time Domain Envelope	98.1711	119.7328	124.3617	100.5270	114.2498	123.7981
Signal Mean inTime Domain	97.4240	119.2350	123.9108	100.0932	113.9132	123.4620
Signal's Standart Deviation in Time Domain	0.4095	0.3075	0.2923	0.2771	0.1930	0.1519
The Peak of Magnitude Spectrum	3.89e5	4.77e5	4.96e5	4.00e5	4.56e5	4.94e6
Average Spectral Side-lobe Energy	17.5696	11.7777	6.1173	2.3928	5.3806	0.7656

Table 3-2: Some Features of Temperature Measurements Just Before Premature Dryout for diameter 254 μm

	Flux 78.9			Flux 276.3		
	1:1	4:1	8:1	1:1	4:1	8:1
Minimum of Time Domain Envelope	101.71	123.71	130.29	102.77	120.33	127.45
Maximum of Time Domain Envelope	104.32	126.08	131.36	103.78	121.11	128.13
Signal Mean in Time Domain	102.93	124.97	130.78	103.42	120.74	127.84
Signal's Standart Deviation in Time Domain	0.71125	0.70236	0.31638	0.25626	0.17674	0.14665
The Peak of Magnitude Spectrum	4.12e5	5.11e5	5.23e5	4.14e5	4.82e5	5.11e5
Average Spectral Side-lobe Energy	136.6046	32.9299	10.7998	9.9706	7.5457	1.2888

Table 3-3: Some Features of Temperature Measurements Before Premature Dryout for diameter 685 μm

	Flux 78.9			Flux 276.3		
	1:1	4:1	8:1	1:1	4:1	8:1
Minimum of Time Domain Envelope	94.5425	116.9045	119.4881	99.6829	131.0437	137.2179
Maximum of Time Domain Envelope	99.6624	121.7385	123.4253	101.8775	132.7440	138.3222
Signal Mean in Time Domain	97.0932	119.3954	121.2495	101.0731	131.8478	137.7478
Signal's Standart Deviation in Time Domain	1.4753	1.4738	0.9818	0.7030	0.4978	0.2867
The Peak of Magnitude Spectrum	4.10e5	4.82e5	4.95e5	4.14e5	5.53e5	5.75e5
Average Spectral Side-lobe Energy	229.6635	260.2009	176.0925	54.4233	29.5581	11.8292

Table 3-4: Some Features of Temperature Measurements Just Before Premature Dryout for diameter 685 μm

	Flux 78.9			Flux 276.3		
	1:1	4:1	8:1	1:1	4:1	8:1
Minimum of Time Domain Envelope	100.28	117.71	121.06	102.42	137.39	143.06
Maximum of Time Domain Envelope	104.95	123.67	127.21	104.9	139.34	144.33
Signal Mean in Time Domain	102.48	120.47	123.68	103.59	138.15	143.65
Signal's Standart Deviation in Time Domain	1.2613	1.3905	1.6386	0.57687	0.45827	0.33587
The Peak of Magnitude Spectrum	10504	14515	15300	10731	19087	20637
Average Spectral Side-lobe Energy	427.0900	694.0514	328.4640	56.2980	94.6943	39.1538

In order to understand the effect of the instability on the temperature frequency spectrum, the Discrete-Time Fourier Transforms (DFT) [78] of temperature readings were determined. N point DFT of $x[n]$ can be written as:

$$X[k] = \sum_{n=0}^{N-1} x[n]e^{-j\frac{2\pi kn}{N}} \text{ for } k = 0,1,...,N-1 \qquad (10)$$

where $j \equiv \sqrt{-1}$, k is the index of the frequency domain sample taken at $f = \dfrac{k}{N}\dfrac{1}{T_s}$ and $X[k]$ represents the corresponding sample of the Fourier Transform , $X(f)$, of the temperature readings (i.e., $X[k] = X(f)\big|_{f=\frac{k}{N}\frac{1}{T_s}}$). In practice, DFT in Eq. (10) can be efficiently implemented by using Fast-Fourier Transform (FFT) [78].

In order to analyze the signal behavior before and just before premature dryout, FFT profiles of the temperature signals are used to see their energy spreads over the frequency for different mass flux densities, restriction ratios and diameters. For this analysis, FFT size N

were taken as 4000, which corresponds to a frequency band of 50 Hz since the sampling periods between time domain samples were 10^{-2} seconds.

To see the effect of the initiation of premature CHF, we first calculate the peak of the magnitude of the spectrum $X[k]$ both before and after the instability as:

$$X_p = \max_{k=0,1,\dots,N-1} |X[k]| \qquad (11)$$

As seen from Figures 3-7 to 3-18, the peak of the magnitude spectrum, X_p, increases consistently under the conditions of impeding premature CHF.

Figure 3-7: Flux 78.9, RR=1:1, diameter 254, temperature FFT profile before premature dryout (on the left) and just before premature dryout (on the right)

Figure 3-8: Flux 78.9, RR=4:1, diameter 254, temperature FFT profile before premature dryout (on the left) and just before premature dryout (on the right)

Figure 3-9: Flux 78.9, RR=8:1, diameter 254, temperature FFT profile before premature dryout (on the left) and just before premature dryout (on the right)
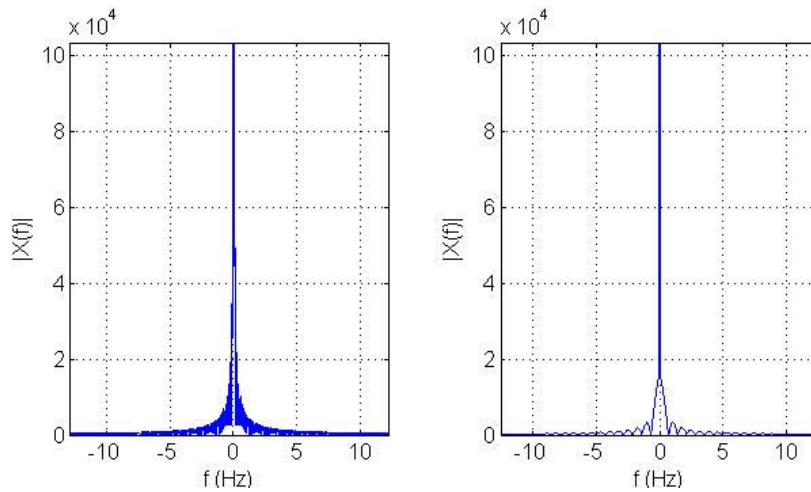
Figure 3-10: Flux 276.3, RR=1:1, diameter 254, temperature FFT profile before instability (on the left) and after instability (on the right)
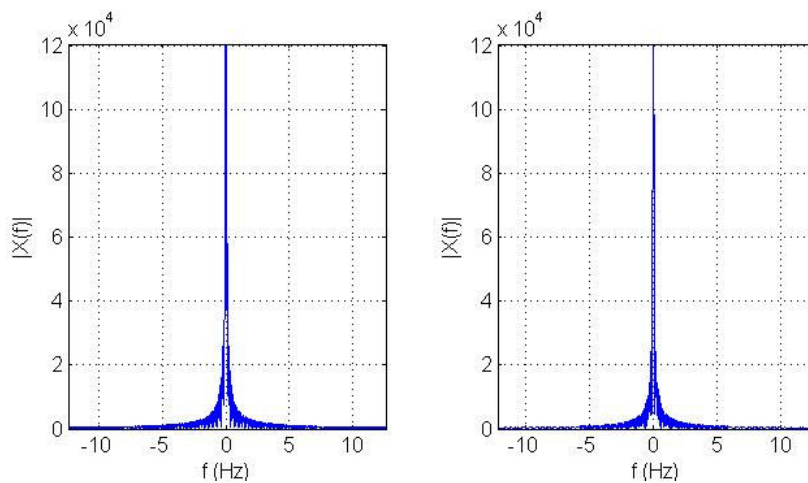
Figure 3-11: Flux 276.3, RR=4:1, diameter 254, temperature FFT profile before premature dryout (on the left) and just before premature dryout (on the right)
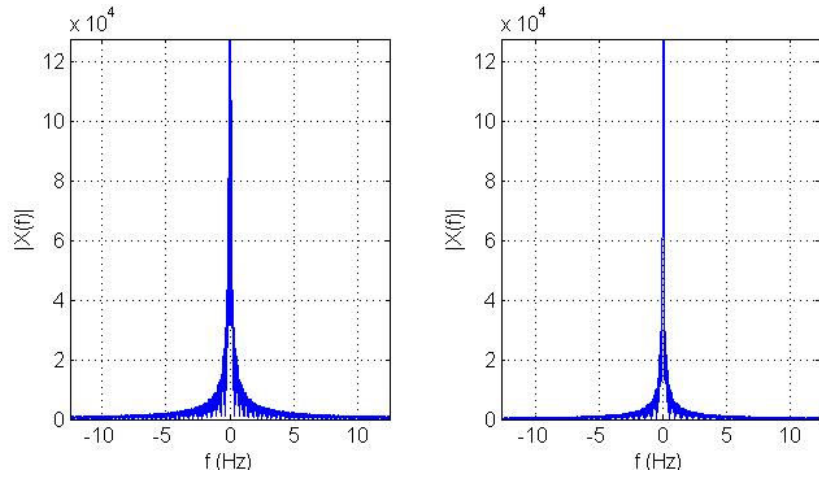
Figure 3-12: Flux 276.3, RR=8:1, diameter 254, temperature FFT profile before premature dryout (on the left) and just before premature dryout (on the right)
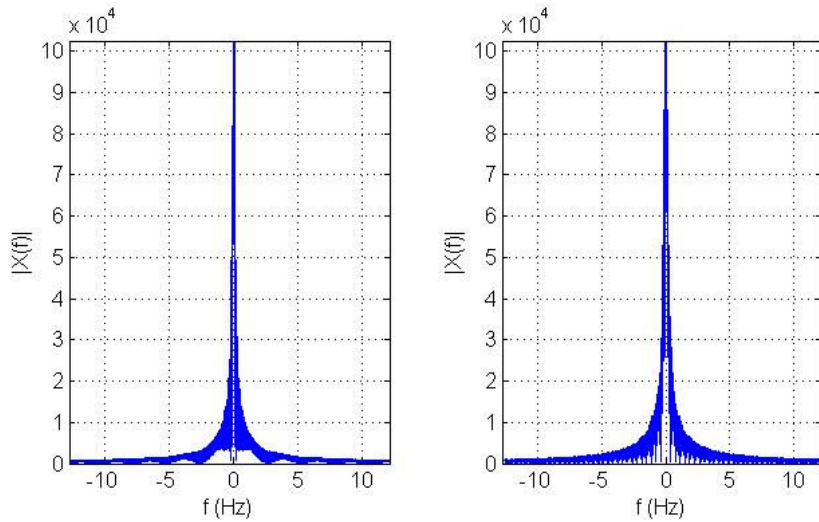
Figure 3-13: Flux 78.9, RR=1:1, diameter 685, temperature FFT profile before premature dryout (on the left) and just before premature dryout (on the right)
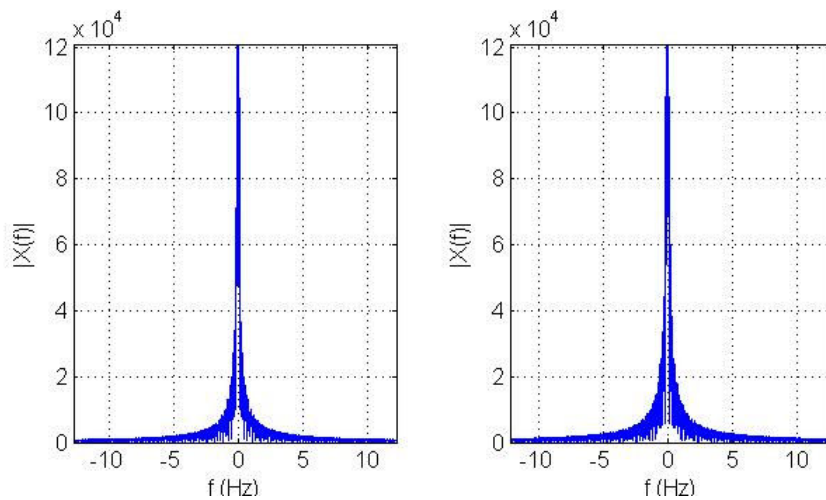
Figure 3-14: Flux 78.9, RR=4:1, diameter 685, temperature FFT profile before premature dryout (on the left) and just before premature dryout (on the right)
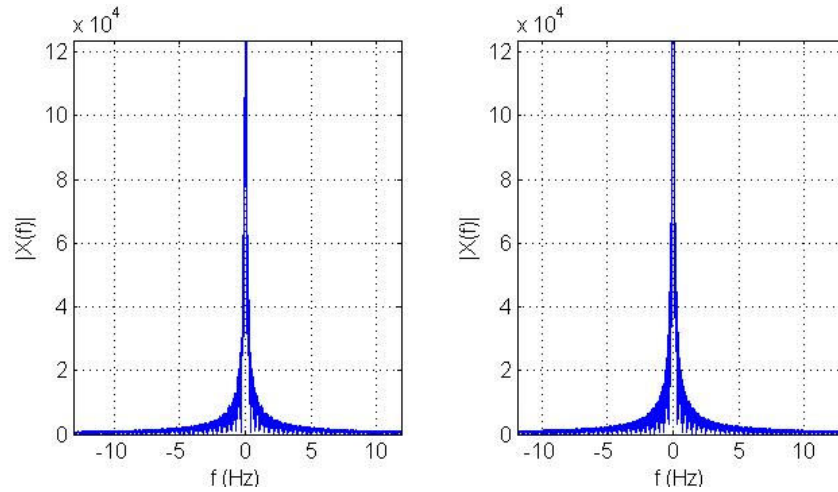
Figure 3-15: Flux 78.9, RR=8:1, diameter 685, temperature FFT profile before premature dryout (on the left) and just before premature dryout (on the right)
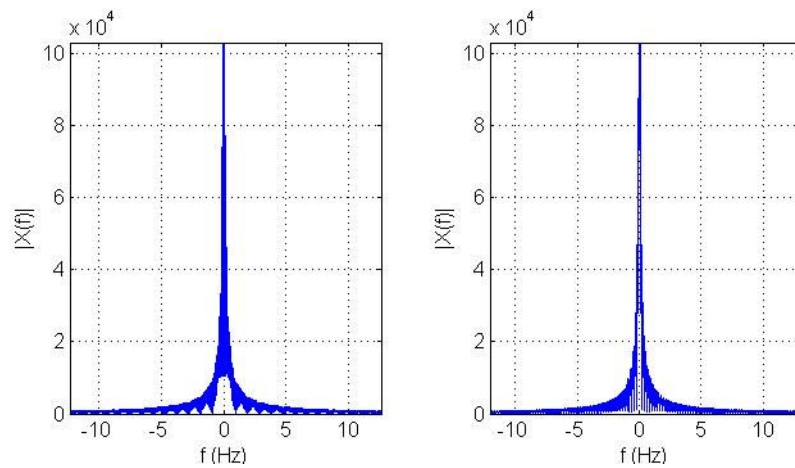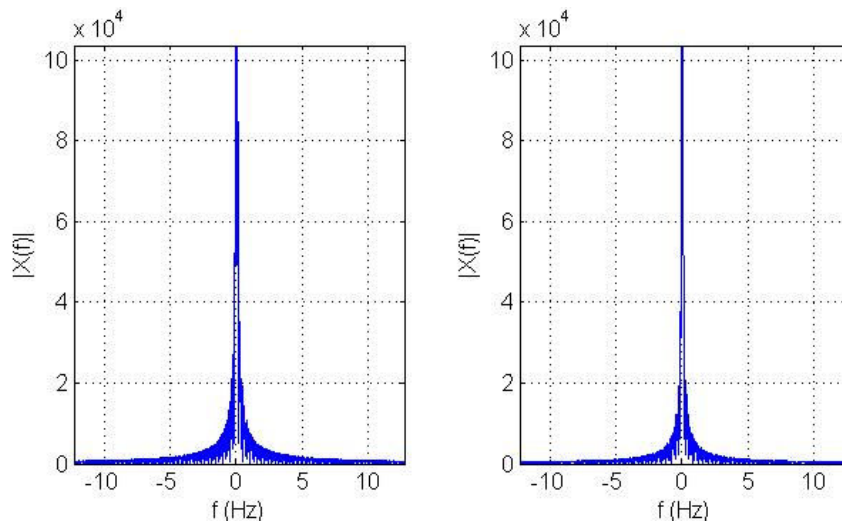

Figure 3-16: Flux 276.3, RR=1:1, diameter 685, temperature FFT profile before premature dryout (on the left) and just before premature dryout (on the right)
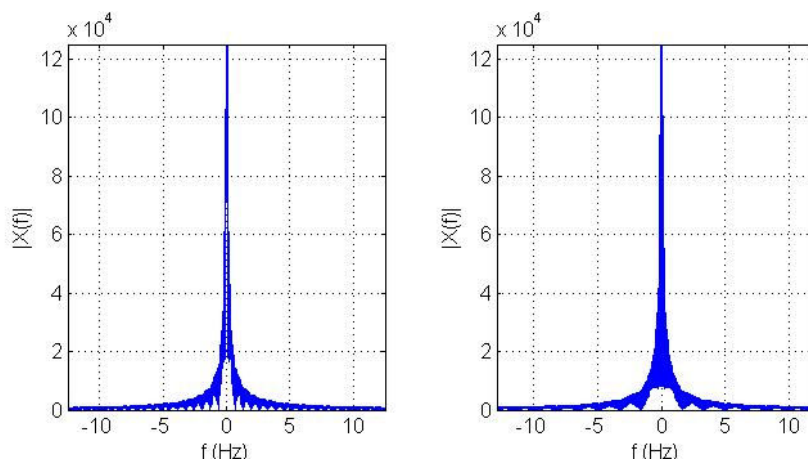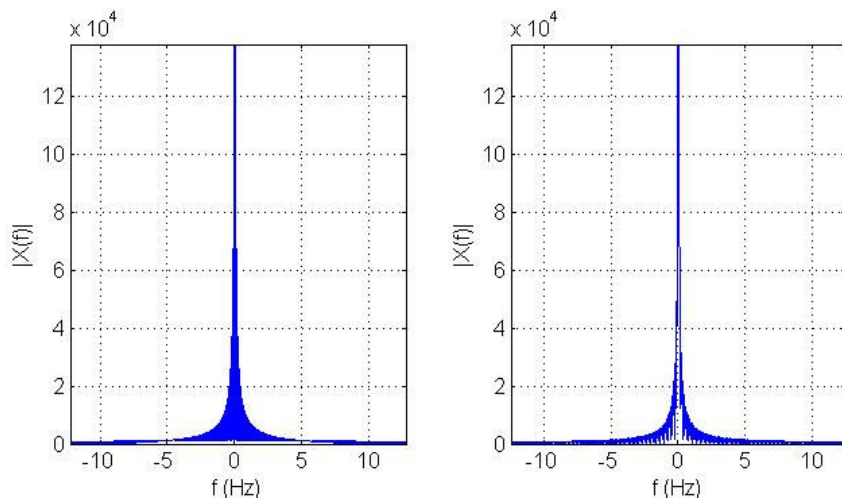

Figure 3-17: Flux 276.3, RR=4:1, diameter 685, temperature FFT profile before premature dryout (on the left) and just before premature dryout (on the right)
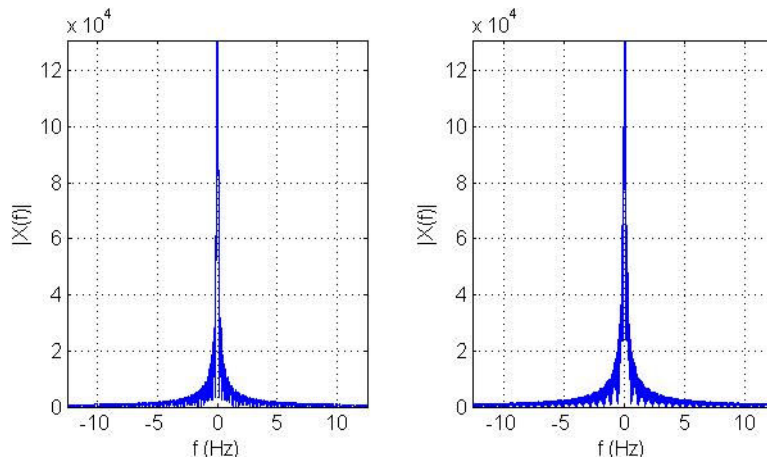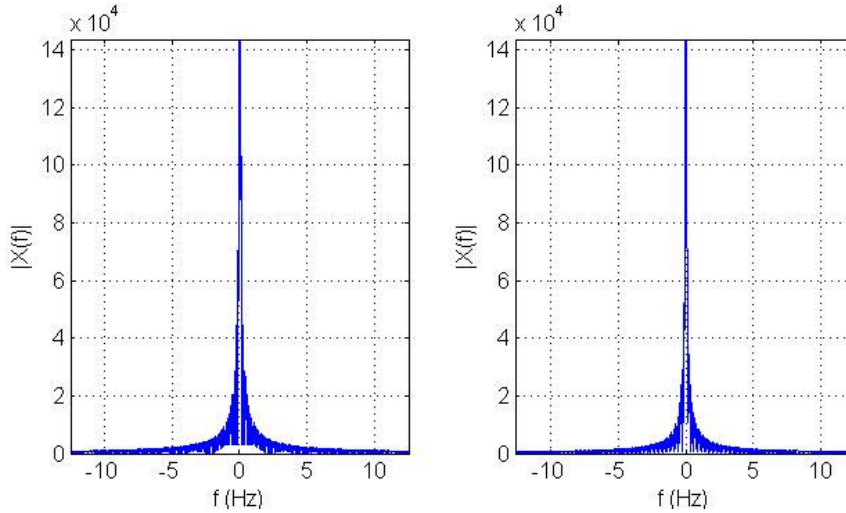
Figure 3-18: Flux 276.3, RR=8:1, diameter 685, temperature FFT profile before premature dryout (on the left) and just before premature dryout (on the right)

In addition to peak of the magnitude spectrum, the mean energy on the side-lobes for each case was observed. To perform this analysis, starting after W_1 frequency samples, first the magnitude spectrum was windowed with a width of length W samples before and after the spectrum peak as illustrated in the Figure 3-19. The spectrum samples within the prescribed window are named as side-lobe samples. Then the mean side lobe energy of can be calculated as:

$$\bar{X}_s = \frac{1}{W} \sum_{k=W_1}^{W_1+W-1} |X[k]|^2 \tag{12}$$

For this experiment, W has been selected as 200, and the windowing has been started after W_1 =30 samples.
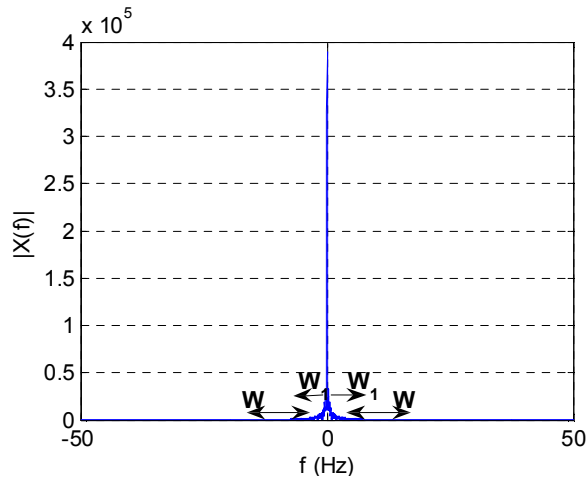
Figure 3-19: Flux 78.9, RR=1:1, diameter 254, temperature FFT profile before premature dryout with windowing

As can be observed from Tables 3-1 and 3-2, under the mass flux value of 78.9 kg/m^{2}s and the diameter size of 254μm, the average size-lobe energy increases just before premature CHF condition by a factor of 6.61, 3.61 and 1.78, respectively, for restriction ratio (RR) of 1:1, 4:1 and 8:1. Using the same size of diameter and the mass flux of 276.3 kg/m^{2}s, it shows an increase by a factor of 1.46, 1.22 and 6.39 for RR of 1:1, 4:1 and 8:1. By employing diameter of size 685 μm, the average size-lobe energy increases by a factor of 2.35, 2.70 and 2.36 for the RR of 1:1, 4:1 and 8:1, respectively, under the mass flux of 78.9 kg/m^{2}s. With the same diameter size and the mass flux of 276.3 kg/m^{2}s, the side-lope energy is boosted by factor of 2.50, 2.04 and 2.18, respectively, for RR of 1:1, 4:1 and 8:1.

These findings suggest that not only the spectrum peak increases significantly but the side-lobe energy also gets drastically higher after the inception of unstable boiling. That implies the high frequency content of the signal which means it changes faster upon the occurrence of premature CHF. Premature CHF mostly occurs suddenly without any significant sign and might lead to catastrophic failure of micro scale devices involving boiling, which imposes serious difficulties in its detection. The drastic change in side-lobe energy just before the occurrence of premature CHF could be exploited as an effective premature CHF detection technique, which could be easily integrated to standard Data Acquisition Systems (DAQ) of boiling heat transfer test setups. When a significant change in side lobe energy occurs, these DAQ systems would act in order to either decrease the input power or to increase the flow rate in the system to avoid premature CHF so that no catastrophic failure would occur in the system.

In order to see the correlation between the pressure level and temperature just before the premature CHF condition has reached, we obtain their scatter plots in Figures 3-20 and 3-21, respectively, for mass flux 276.3 kg/m^{2}s, RR=1:1, diameter 254 μm and mass flux 78.9 kg/m^{2}s, RR=4:1, diameter 685 μm as samples.
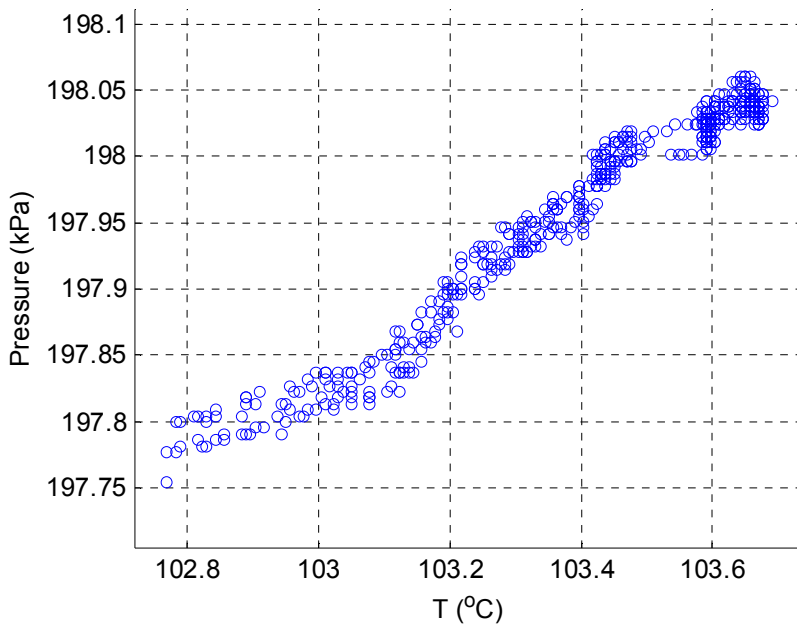
Figure 3-20: Flux 276.3, RR=1:1, diameter 254, Scatter plot of temperature versus pressure change just before premature
1dryout
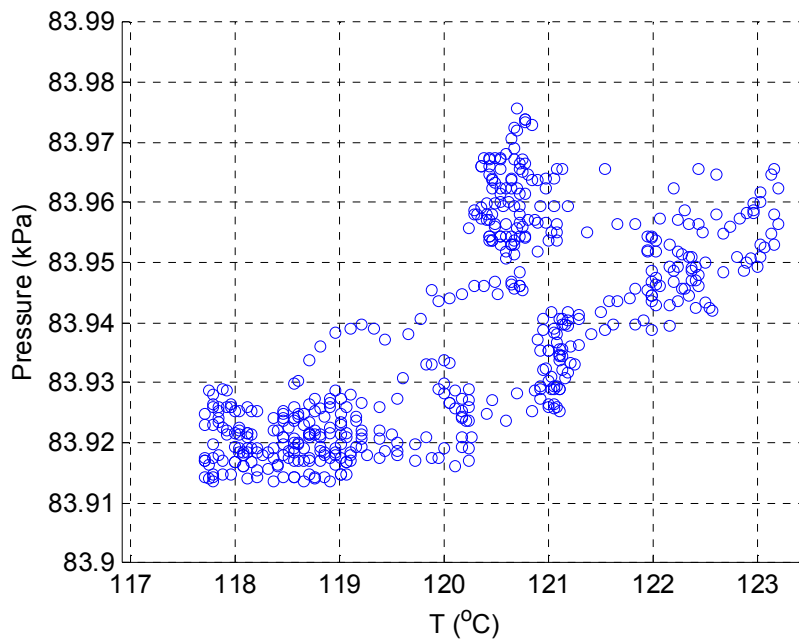
Figure 3-21: Flux 78.9, RR=4:1, diameter 685, Scatter plot of temperature versus pressure change just before premature
dryout

These scatter plots suggest that the pressure level and temperature just before premature CHF conditions are highly correlated. To better understand this, their cross-correlation can be calculated as:

$$\rho_{xy} = \frac{\frac{1}{N}\sum_{n=1}^{N}(x[n]-\overline{x})(y[n]-\overline{y})}{\sigma_x \sigma_y} \qquad (12)$$

where $x[n]$ and $y[n]$ represent the temperature reading and the corresponding pressure respectively, $\overline{x}, \overline{y}$, σ_x and σ_y denote the mean of $x[n]$, the mean of $y[n]$, the standard deviation of $x[n]$ and the standard deviation of $y[n]$. ρ_{xy} as 0.86 and 0.71 were determined respectively for mass flux 276.3 kg/m^{2}s, RR=1:1, diameter 254 μm and for Flux 276.3 kg/m^{2}s, RR=1:1, diameter 254 μm, which clearly shows such as high correlation between temperature and pressure signals, and thus, proves that pressure and temperature fluctutions have similar characteristics and have similar sources.

3.2 Second Part - Ultra High Mass Flux Flow Boiling

Critical heat flux results for high mass flux flow boiling de-ionized water in ~249 μm and ~494 μm inner diameter tubes that are heated along short heated lengths (2-10 mm, 7.6<L_h/d_i<39.4). The corresponding exit mass qualities vary from -0.1 to 0.06. Due to low mass qualities and high mass fluxes (>20000 kg/m^{2}s), it is very likely that the critical heat flux condition is associated with departure from nucleate boiling (DNB).

3.2.1 Parametric effects

In Fig. 3, the critical heat flux is shown as a function of mass velocity at fixed diameter and heated lengths. Similar to the findings in the literature [79-82], CHF has an increasing trend with mass velocity over the entire mass velocity range for all channel diameters. Growing bubbles, bubbles crowding channel surfaces, and slugs or vapor clots are possible scenarios for triggering DNB type CHF conditions. It is more likely that they can be removed more easily at higher flow rates leading to more effective liquid replenishment to the channel wall thereby delaying CHF condition to higher heat flux values. The trend of the CHF data has a linear relationship with mass flux (CHF~$G^{1.1}$), whereas a weaker dependence on mass

velocity was reported in some other conventional channels studies [79-82]. The stronger mass flux effect, which was also observed in the study of Koşar et al. [83] on micro scale flow boiling, might be explained by possible bubble-to-channel interactions. For small channels diameter ratio could be relatively large, and emerging bubbles could occupy a significant portion of the tube cross-section leading to a negative effect on the liquid supply to the heated wall. This ratio diminishes with increasing mass flux, which results in increasing rate of CHF increase. As a result, a higher power law dependency of the CHF on mass velocity is present compared to conventional scale. Moreover, the slope of the profiles has a decreasing trend with increasing diameter suggesting a higher dependency on mass flux in smaller scales.
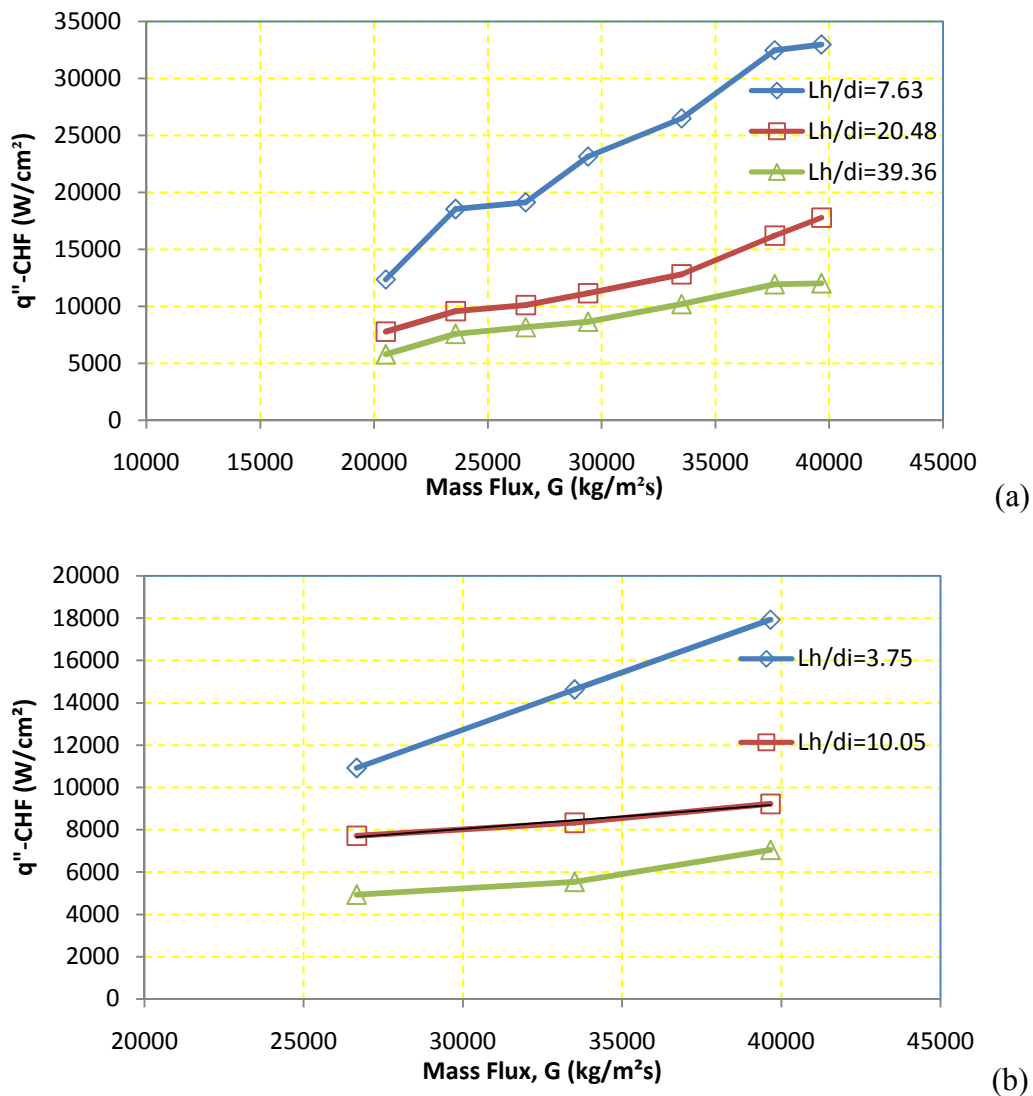
Figure 3-22: Effect of mass velocity on CHF (a) smaller diameter (b) larger diameter.

Figure 4 displays the trend in CHF with length over diameter ratio. Most conventional scale studies emphasize that the heated length is an important independent variable for $L_h/d_i < 50$

40

[18, 84], and CHF has a decreasing trend with increasing length at fixed mass flux, which constitutes the motivation of the current study for having higher CHF values with short heating lengths. As seen from Figure 3-22, the general trend observed in the current study having L_h/d_i values less than 40 is consistent with previous studies. The dependence of CHF on L_h/d_i seems to be in the same level as in the past studies (Sarma et al., $\sim(L_h/d_i)^{-0.58}$). The L_h/d_i effect is a conjugate effect of other flow parameters including channel diameter, subcooling, mass velocity, and diameter [49]. The contributions from these flow parameters result in a decreasing trend in CHF with increasing Lh/d_i consistent with literature.
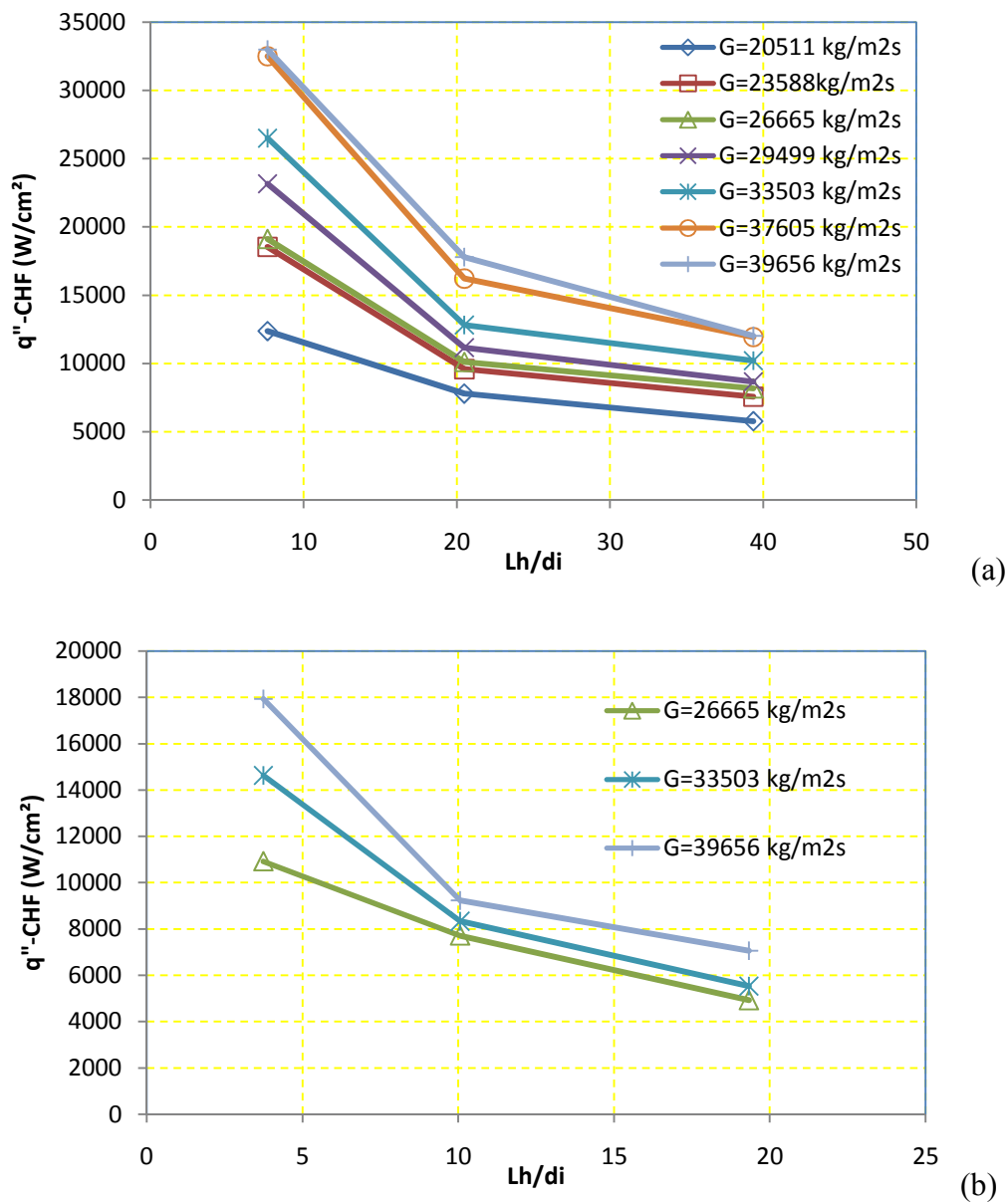
Figure 3-23: Effect of heated length on CHF (a) smaller diameter (b) larger diameter.

41

The effect of diameter was investigated by various researchers in the literature [45, 50]. Accordingly, CHF increases with decreasing tube diameter. This effect becomes less significant for tube diameters above 5 mm size so that beyond a certain tube size (8mm for Groeneveld [50]) CHF is insensitive to the diameter. In Figure 3-23 the comparisons can be seen at fixed L_h/d_i ratio and mass velocity. CHF is inversely related to channel diameter over the entire mass flux range consistent with the CHF trend of Vandervort et al. [47] and most of the data of Koşar et al. [43]. Significant increase in CHF (more than 100%) with a reduction of 50% in size could generate high heat flux values (larger than 30000W/cm^2) particularly at low L_h/d_i ratios, which could be exploited in nano-scale plasmonic applications, near field radiative energy exchange between objects, nano thermophotovoltaics, where localized small scale cooling is necessary and integrated with small scale heating. For example, when wall superheats at CHF condition are assumed to be 100°C, the corresponding heat transfer coefficient has a value of 4.2x10^6 W/m^{2o}C, which is a desired heat transfer coefficient in nano TPV application for maximizing the efficiency [44]. According to the normalization of CHF relative to CHF in an 8 mm tube suggested by Groeneveld [50], the exponent of the power law is -0.5, whereas a higher dependency is evident in the current study ($\sim d_i^{-2}$). This stronger dependence on tube diameter could be associated with possible bubble-to-channel interactions as in mass flux. For small channels diameter ratio could be relatively large, and emerging bubbles could occupy a significant portion of the tube cross-section leading to a more pronounced effect of diameter on CHF.
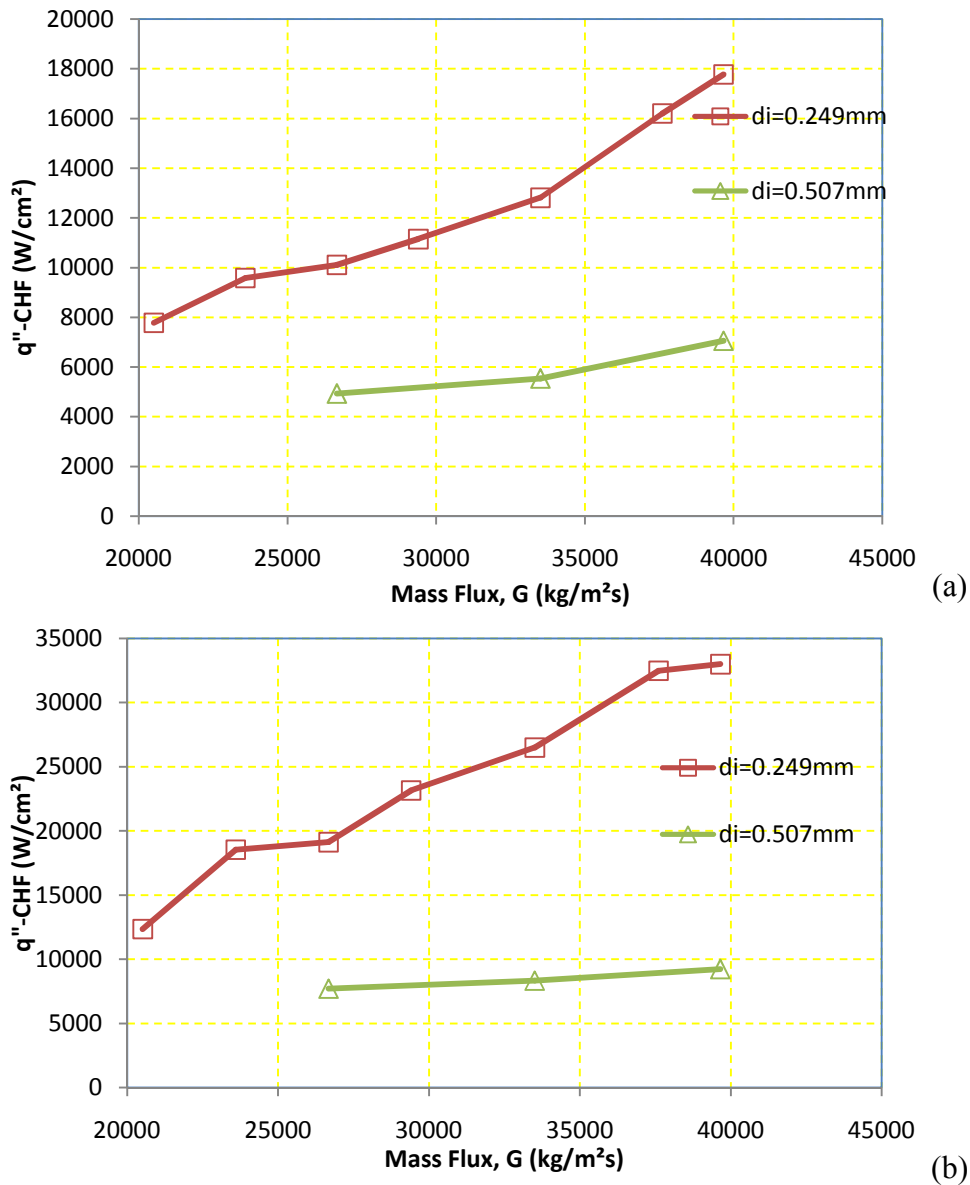
Figure 3-24: Effect of the inner diameter on CHF (a) $L_h/d_i \sim 20$ (b) $L_h/d_i \sim 8$.

3.2.2 Comparison with Existing Correlations and Development of CHF Correlations Recommended For both Conventional and Small Scale Channels

The CHF data obtained in the present study are compared to one general commonly used correlation developed for conventional channels, one general correlation developed for small channels, one supercorrelation for small channels having large length over diameter ratio (>50), and one general correlation developed for microchannels (see Table 3-5).

Katto and Ohno [51] have developed for saturated flow boiling, while Sarma et al. [52] correlation was recommended for small channels. The supercorrelation of Koşar et al. [53] was developed for small channels with relatively high L_h/d_i values. The prediction tool suggested by Kandlikar [42] provides estimation for saturated CHF in microchannels and consists of subcorrelations depending on working conditions.

The comparison between the experimental data and Katto and Ohno correlation [51] is shown in Figure 3-25. A large deviation between the correlations and the current experimental data is evident particularly for smaller size tube. This correlation generates an MAE of 31.7%, while its prediction shows a significant improvement in prediction for larger size channel (MAE of 14.3%). The large size tube experimental data could be predicted within ±30% by this correlation. A better performance in prediction is expected since this correlation was recommended for a CHF database having a minimum channel size of 1mm. The experimental data corresponding to small diameter tube is underpredicted by this correlation, which could be attributed to enhancing effects of micro scale tubes on CHF discussed in the previous section, which could not be capture by this correlation.
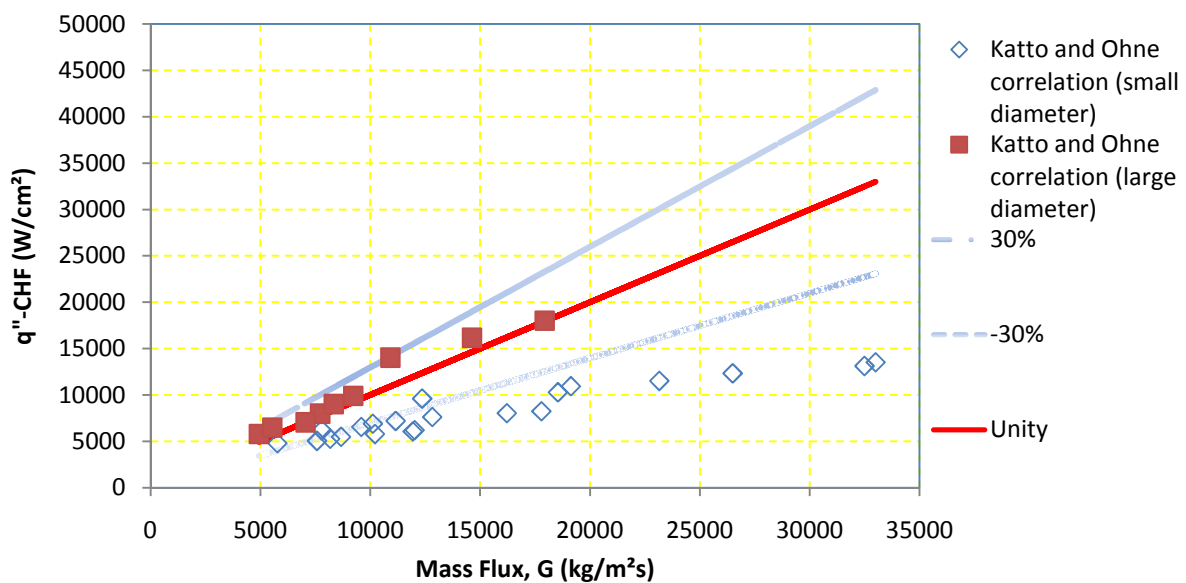
Figure 3-25: Comparison between the experimental data and Katto and Ohno correlation [51]

The Sarma et al. [52] correlation recommended for small channels predicts the data with a MAE of 56% (Figure 3-26). Most of the data is underpredicted by this correlation. Since the lowest channel size in the CHF data base considered in this correlation is 0.25 mm, and the number of data points at smaller size was limited and L_h/d_i values in the database were

mostly larger than 10, enhancing effects of smaller scale and short tubes on CHF could have possibly played a role in this underprediction. For larger size tubes, the prediction is improved as expected (MAE of 39%).
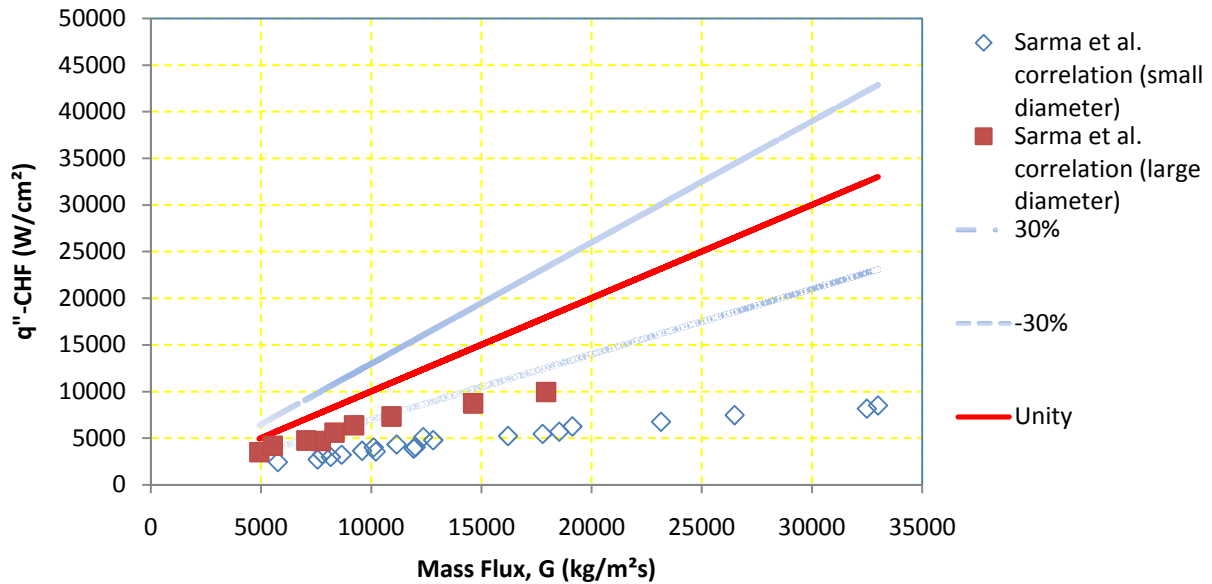
Figure 3-26: Comparison between the experimental data and Sarma et al. correlation [52]

Figure 3-27 shows the prediction of the supercorrelation of Koşar et al. [53], where their experimental data together with the CHF data of Bergles [45] and Vandervort et al. [81] were considered. The database mostly consisted of CHF data from channels of relatively L_h/d_i values (>20). This supercorrelation predicts the experimental data with an MAE of 39.5%, while the data while data corresponding to low L_h/d_i values(<10) is underpredicted, which is not suprising due to the the inverse relationship of CHF with L_h/d_i ratio. However, for higher L_h/d_i values a beter prediction is evident, where most of the data could be predicted within ±30% by this correlation (MAE =28%).
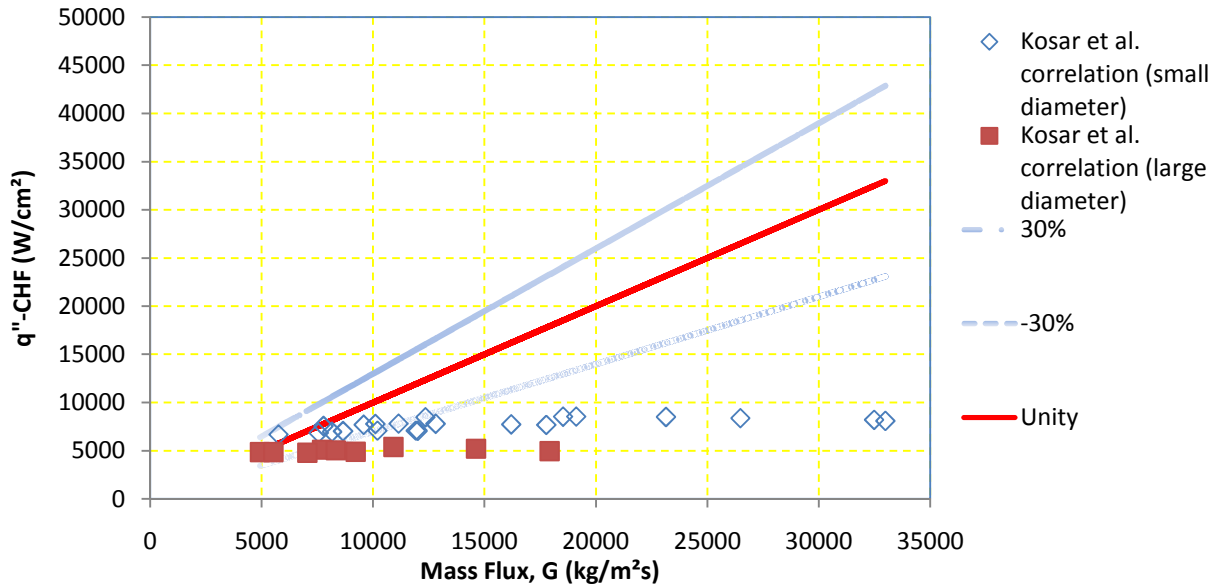
Figure 3-27: Comparison between experimental data and Koşar et al. correlation [53]

For the comparison between the experimental data and the method of Kandlikar [47], which is developed for a large database consisiting of almost all the available CHF data in micro scale, the data corresponding to exit qualities greater than zero are taken, and the appropriate subcorrelation in this method is chosen. Figure 3-28 shows the fair prediction of this method. As seen from this figure, the predicted CHF values fall within ±30% of the experimental data, and the resulting MAE is 24% proving its applicability to a wide variety of working conditions for the prediction of CHF in microchannels.
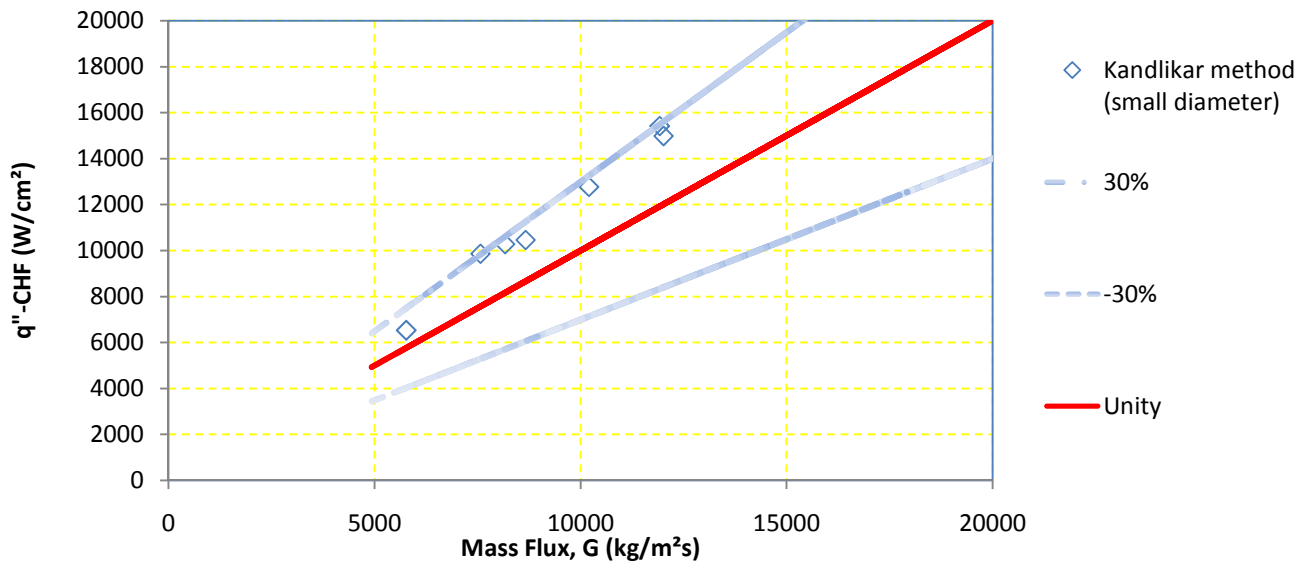
Figure 3-28: Comparison between experimental data and Kandlikar's correlation [47]

The experimental data are used to develop a correlation providing the best prediction of the experimental data based on Curve Fitting using Least Squares Method. This correlation is based on the approach of Sarma et al. [52], where CHF is expressed as a function of diameter, length over diameter ratio and mass flux, and is expressed as:

$$q''_{CHF}=1.203 \text{x} 10^{-4} \frac{\mu_L h_{FG}}{d_i^{1.42}} \text{Re}^{1.28} \left(\frac{p_e}{p_{cr}}\right)^{0.2} \left(\frac{L_h}{d_i}\right)^{-0.58} \left(\frac{c_{p.e}\Delta T_{subi}}{h_{Fg,e}}\right)^{0.216} \qquad \text{(in W/m}^2) \qquad (13)$$

The above correlation has an MAE of 5.7% to the current CHF data (30 data points, G>20000kg/m2s) with x_e<0.1. All of the experimental data are within ±10% of the correlation.
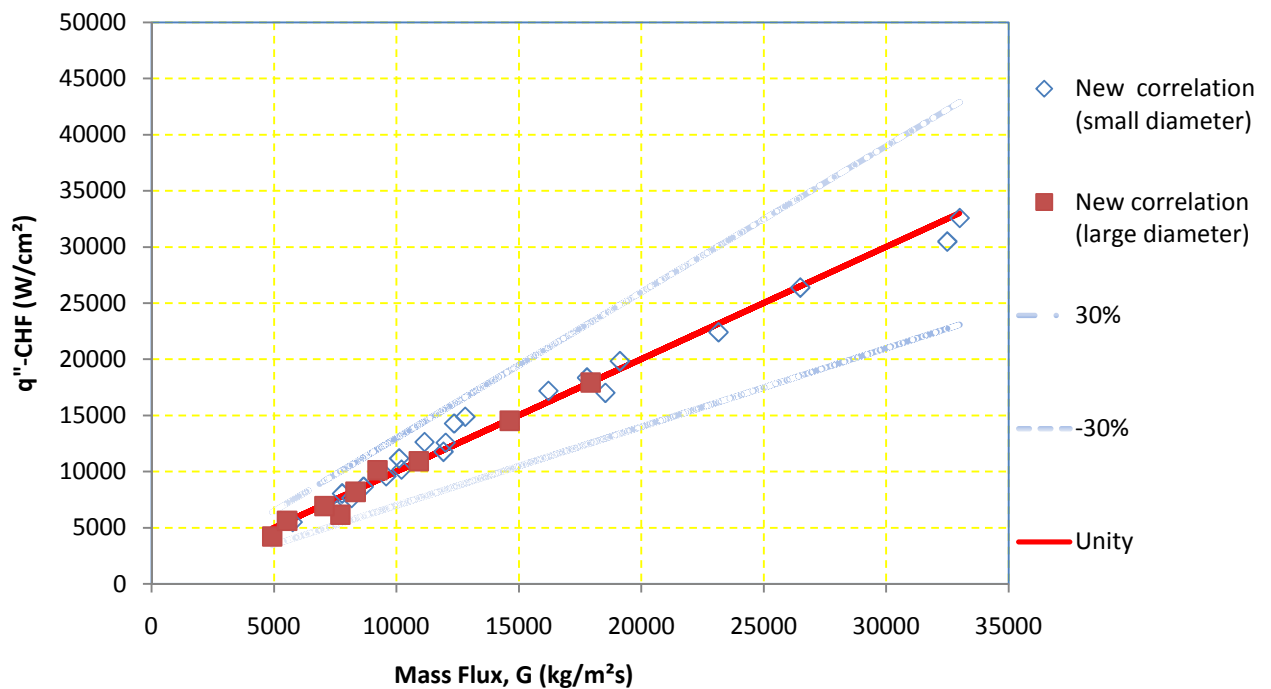
Figure 3-29: Comparison between experimental data and correlation

Table 3-5: Subcooled/low quality CHF correlations

Correlation number	Reference	Recommended conditions	Correlation
1	Katto and Ohno [51]	Circular, conventional channels, low quality version	$q''_{CHF} = XG\big(h_{FG} + K(\Delta h_{sub})_i\big)$ where $X_1 = \dfrac{0.1\left(\rho_G/\rho_F\right)^{0.133}\left(\dfrac{\sigma \rho_F}{G^2 L_h}\right)^{0.333}}{1.0 + 0.0031(L_h/d_i)}$ $X_2 = \dfrac{0.098\left(\rho_G/\rho_F\right)^{0.133}\left(\dfrac{\sigma \rho_F}{G^2 L_h}\right)^{0.433}(L_h/d_h)^{0.27}}{1.0 + 0.0031(L_h/d_h)}$ $K = \dfrac{0.833(0.0124 + d_h/L_h)}{\left(\dfrac{\rho_G}{\rho_F}\right)^{0.133}\left(\dfrac{\sigma \rho_F}{G^2 L_h}\right)^{0.333}}$ (MAE of 14.3%) $X=X_1$ if $X_1<X_2$ and $X=X_2$ if $X_2<X_1$
2	Shah [23]	Circular, conventional channels, low quality version	$q''_{CHF} = 0.124 G h_{FG} \left(\dfrac{d_h}{L_h}\right)^{0.89}\left(\dfrac{10^4}{Y}\right)^{n}(1-x_i)$ where $n = \dfrac{0.12}{(1-x_i)^{0.5}}$; $Y = \left(\dfrac{G d_i c_{p,F}}{k_F}\right)\left(\dfrac{G^2}{\rho_F^2 g d_i}\right)^{0.4}\left(\dfrac{\mu_F}{\mu_G}\right)^{0.6}$ (MAE of 39%)
3	Sarma et al. [52]	Small channels, DNB type CHF	$q''_{CHF} = 0.118 \dfrac{\mu_L h_{FG}}{d_i} \mathrm{Re}^{0.77}\left(\dfrac{p_e}{p_{cr}}\right)^{0.2}\left(\dfrac{L_h}{d_i}\right)^{-0.45}\left(\dfrac{c_{p,e}\Delta T_{sub,i}}{h_{Fg,e}}\right)^{0.216}$ (MAE of 28%)
4	Kandlikar [42]	Microchannels CHF for Saturated Boiling for both low and high exit qualities	$K2,CHF = a1(1 + \cos\theta) + a2\ We(1-x) + a3\ Ca(1-x)$ where $a1 = 1.03\text{x }10^{-4}$ $a2 = 5.78\text{x }10^{-5}$ (MAE of 24%) $a3 = 0.783$
5	Koşar et al. [53]	Microtubes CHF for low exit qualities, high mass fluxes and large length over diameter ratios	$q''_{CHF}=a_o\big(d_i^{(a_1+a_2 d_i+a_3(L_h/d_i)+a_4 G+a_5 p_e+a_6(T_{sate}+\Delta T_{sube}))}\big)\left(\dfrac{L_h}{d_i}\right)^{(a_7+a_8 d_i+a_9(L_h/d_i)+a_{10}G+a_{11}p_e+a_{12}(T}$ $(G^{(a_{13}+a_{14}d_i+a_{15}(L_h/d_i)+a_{16}G+a_{17}p_e+a_{18}(T_{sate}+\Delta T_{sube}))})(p_e^{(a_{19}+a_{20}d_i+a_{21}(L_h/d_i)+a_{22}G+a_{23}p_e+a_{24}(T_{sate}+\Delta T_{sube})})$ $\big((T_{sate}+\Delta T_{sube})^{(a_{25}+a_{26}d_i+a_{27}(L_h/d_i)+a_{28}p_e+a_{29}p_e+a_{30}(T_{sate}+\Delta T_{sube}))}\big)$ (MAE of 39.5%)

Table 3-6: Dimensionless parameters in Correlation 5

Variable	Value	Variable	Value	Variable	Value
a_0	1597831	a_{11}	-3.047E-04	a_{22}	1.529E-05
a_1	-1.599	a_{12}	1.863E-03	a_{23}	6.802E-04
a_2	-2.114	a_{13}	0.478	a_{24}	-1.187E-02
a_3	2.611E-03	a_{14}	-1.266E-02	a_{25}	-4.888
a_4	-7.361E-08	a_{15}	-1.909E-04	a_{26}	0.975
a_5	3.265E-04	a_{16}	-7.493E-06	a_{27}	-7.617E-04
a_6	-4.017E-03	a_{17}	-1.407E-04	a_{28}	-6.728E-07
a_7	-0.419	a_{18}	-1.269E-03	a_{29}	-3.583E-04
a_8	-5.025E-03	a_{19}	1.571	a_{30}	1.686E-02
a_9	-6.553E-04	a_{20}	-0.138		
a_{10}	3.292E-06	a_{21}	1.761E-03		

3.3 Part Three - High Mass Flux Flow Boiling on Nanostructre Coated Microchannels

3.3.1 CHF Enhancement Results

In Figures 3-30 and 3-31, the experimental data of heat flux are shown with wall superheat plain and pHEMA coated microchannels having three different hydraulic diameters (~ 250 µm, 500 µm and 1 mm) at two high mass flux values (G=10000 kg/m^{2}s and G=13000 kg/m^{2}s). The heated length subjected to Joule heating was 2 cm. The value range of exit mass qualities for the performed experiments is between -0,28 to -0,17. The negative value of the exit quality implies that the boiling condition is subcooled flow boiling [85], and the occurred CHF mechanism is most likely to be DNB type [46].

In Figure 3-30, the comparison in boiling curves between the plain surface tube and the nanostructured tube for the mass flux value of 10000 kg/m^{2}s can be observed, where the CHF enhancement via pHEMA coating in microchannels having various diameters is shown. The

coated pHEMA provided a CHF enhancement of CHF 17% for the 249 μm tube, of 24% for the 500 μm, of 8% for the 1mm microtube, respectively.
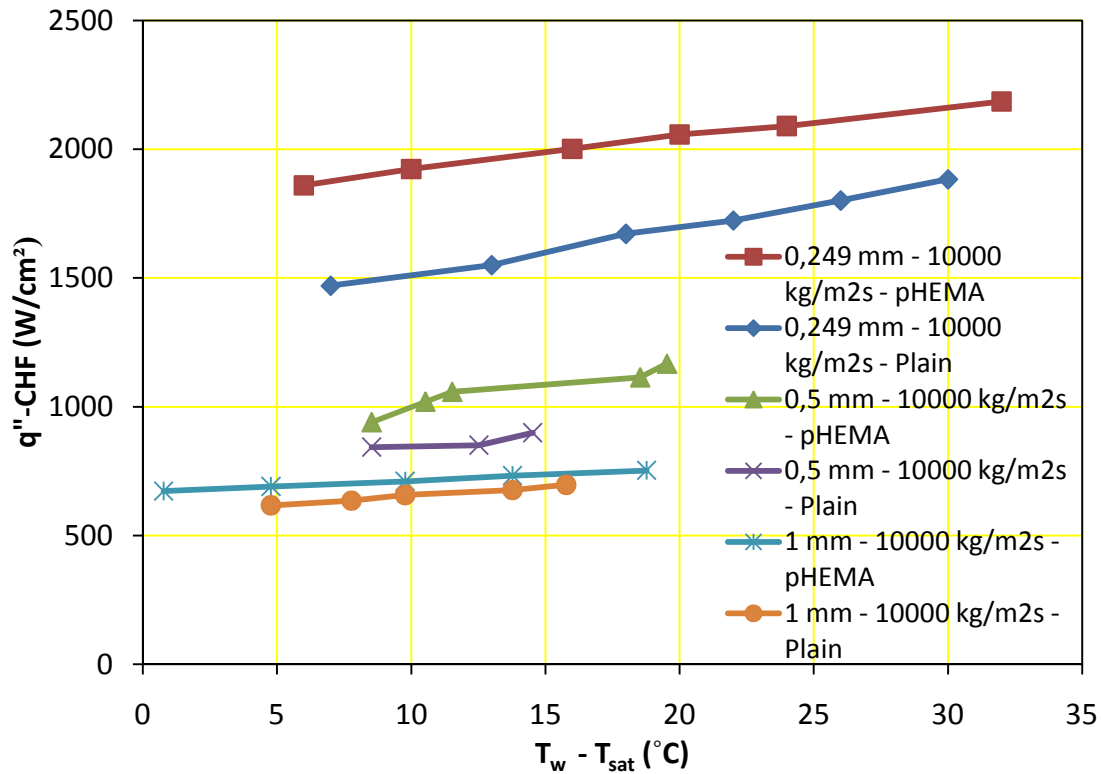
Figure 3-30: Boiling curve for 10000 kg/m^{2}s

The Figure 3-31 shows boiling curves performance of for different microchannel diameters at the mass flux value of 13000 kg/m^{2}s. The enhancement ratio in this case is observed to be 18% for the 249 μm tube, 22% for the 500 μm, and 17% for the 1mm microtube, respectively.
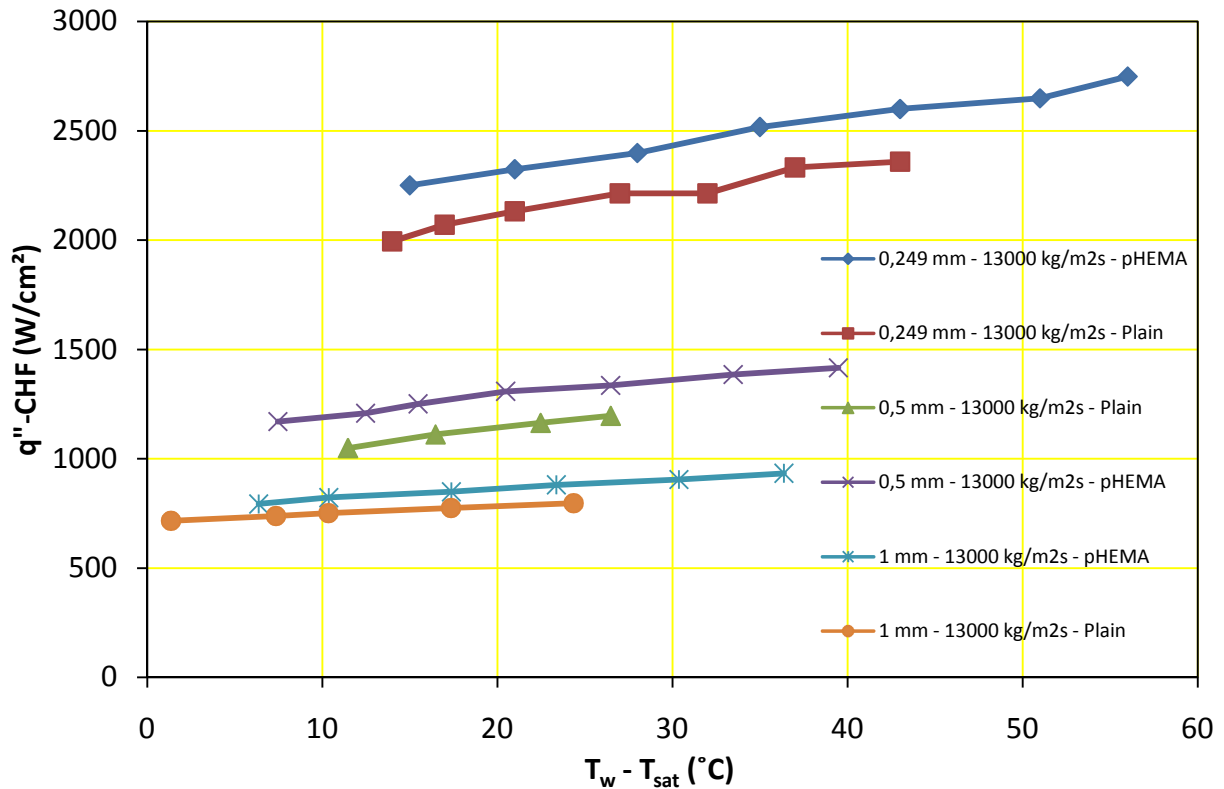
Figure 3-31: Boiling curve for 13000 kg/m^{2}s

When T_w (°C) comparison with the plain microtubes is made, at $G = 10000$ kg/m^{2}s, the coated pHEMA showed ~5% increase in 249 μm tube, ~8% in 500 μm tube and ~6% in 1 mm tube. For the case of $G = 13000$ kg/m^{2}s the ratio of enhancement was ~5% increase in 249 μm tube, ~8% in 500 μm tube and ~8% in 1 mm tube. According to these experimental results, the swelling property and low contact angle (~20°, Trujillo et al. [86] , Chan and Gleason [87]) of pHEMA coated by iCVD on micro channel inner walls has a significant effect in enhancing the CHF value, especially at tube diameters below 1 mm. The proposed extra wetting layer on the inner tube walls helped the channel's heated surface to achieve higher temperatures, by overcoming the insulation caused by the vapor blanket located at the periphery of the bulk fluid. On the other hand, nanostructures on the tube walls have a significant effect in heat removal. The aforementioned studies [62, 64-68] have a similar principle of flow boiling investigation from the aspect of nanostructure coating on microtube walls. The increased amount of heat transfer area by the coated pHEMA nanostructures could be a supplementary factor that increases the heat transfer rate, thus the CHF eventually.

Moreover, according to Figures 3-30 and 3-31, the CHF value significantly decreases as the hydraulic diameter increases. The effect of diameter deduced from the experimental results demonstrates accordance with the literature in related issue [86, 87]. At smaller diameters, CHF value was observed to be equal to 300% of the values at microchannels having 1 mm hydraulic diameter. As Koşar et al. [31] mentioned in their study, the reason behind this strong dependence in small scales could be due to bubble-to-channel interactions, where the formed bubbles occupy more space inside the microtube and therefore the effect on CHF is enhanced.

Furthermore, the CHF enhancing effect of increasing mass flux can be clearly seen by comparing the previous Figs. 3-30 and 3-31. There are studies in the literature that report the linear relationship between CHF and mass flux for conventional scales [32-34]. However, the mass flux gains more importance as the scale becomes smaller. Since the DNB type CHF occurs due to vapor formations at the microtube walls, the effect becomes more significant as the bubble size/channel diameter ratio increases. For overcoming the premature CHF at small scales, increasing the mass flux could be effective by causing liquid replenishment on the tube walls [48].

3.3.2 Boiling Heat Transfer Results

Figures 3-32 to 3-35 display two phase heat transfer coefficients obtained from the tested microtubes. As seen from the figures, very high heat transfer coefficients (>200000 W/m^{2}K) can be achieved with flow boiling in microscale at high flow rates, implying that this method could be exploited in new emerging technologies such as nano-scale plasmonic applications, near field radiative energy exchange between objects, nano thermophotovoltaics.

Figures 3-32 & 3-33 display the dependence of heat transfer coefficient on mass flux. With the increase in mass flux, heat transfer coefficient has an increasing trend. Due to this strong dependence, it could be stated that convective boiling effects are dominant. Moreover, strong size effects are also evident in these figures. An inverse relationship between heat transfer coefficient and microtube size can be observed, which is in agreement with the literature [46].

An enhancement with nanostructures in heat transfer is observed from Figures 3-32 to 3-35. This could be attributed to enhanced nucleate boiling in nanostructured tubes, where suitable

spots are offered for active nucleation sites with nanostructures contributing together to bubble nucleation. The porous structures generated by nanostructures also serve for capillary wicking, which mitigates liquid replenishment after bubble departure, and further contributes to boiling heat transfer. As a result, an increase of 202% for 250 micron tube at G=10000 kg/m^{2}s, 112% for 250 micron tube at G=13000 kg/m^{2}s, 19% for 500 micron tube at G=10000 kg/m^{2}s, 15% for 500 micron tube at G=13000 kg/m^{2}s, 5% for 1 mm tube at G=10000 kg/m^{2}s, 10% for 1mm tube at G=13000 kg/m^{2}s could be attained with nanostructure surface at fixed mass velocity and exit qualities.
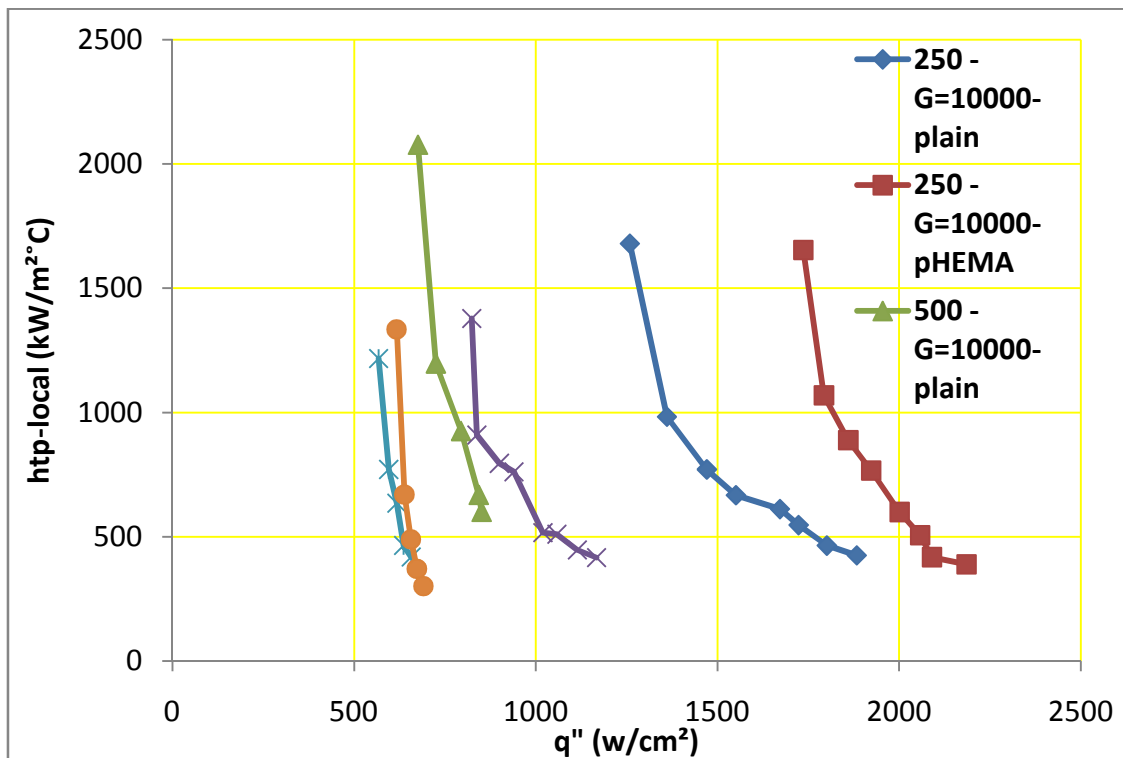

Figure 3-32: Heat transfer coefficient vs Heat Flux for G = 10000 kg/m^{2}s
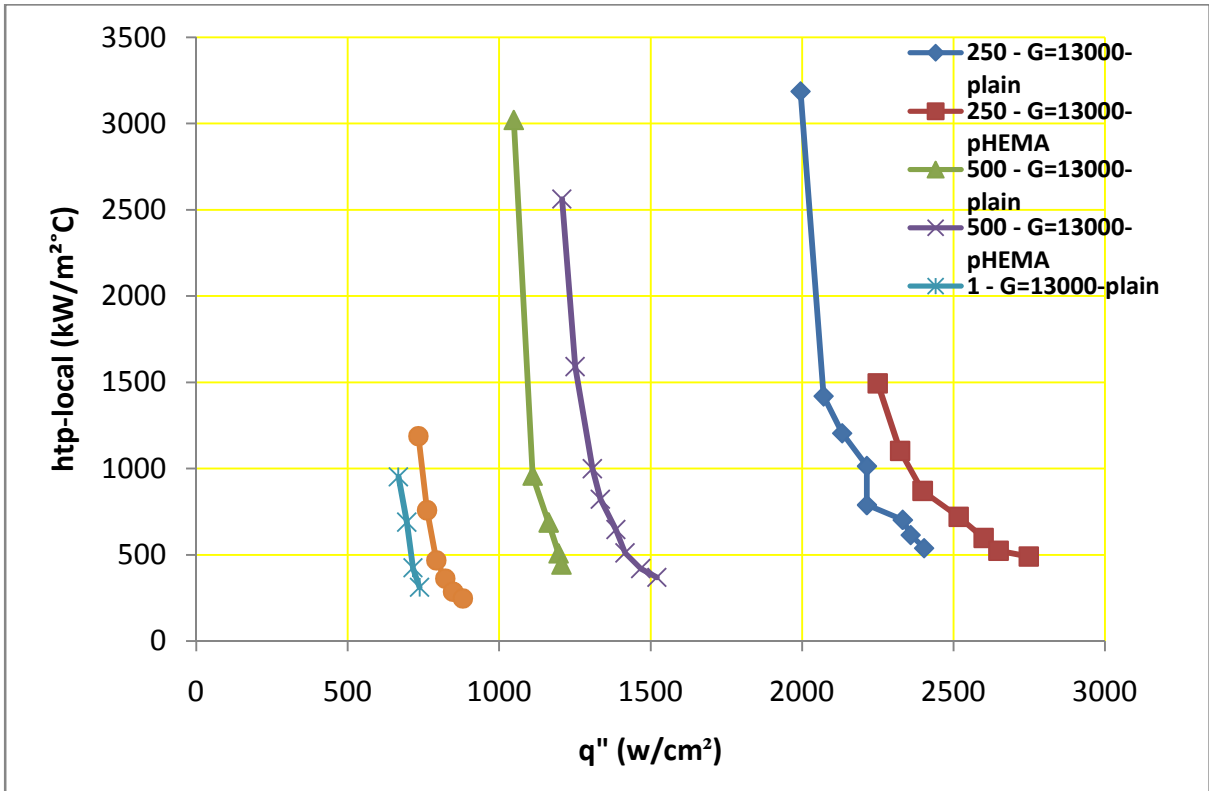
Figure 3-33: Heat transfer coefficient vs Heat Flux for G = 13000 kg/m^{2}s
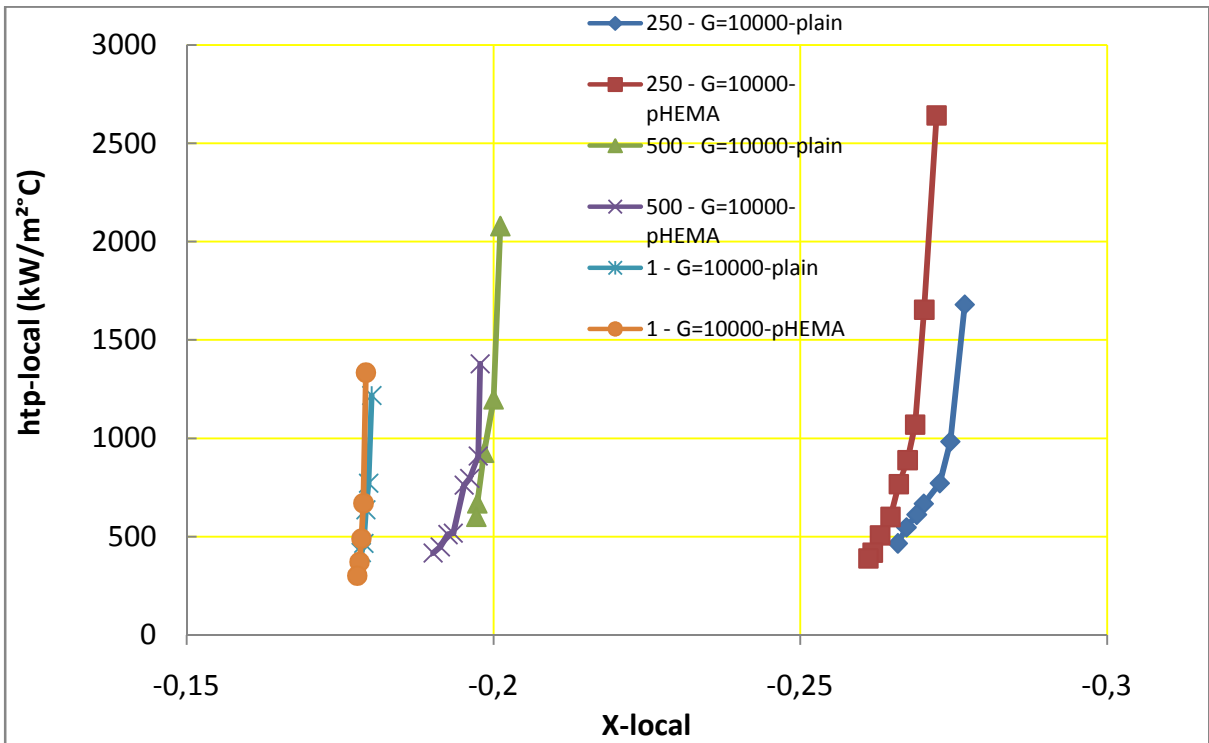
Figure 3-34: Heat transfer coefficient vs X_{kocal} for G = 10000 kg/m^{2}s
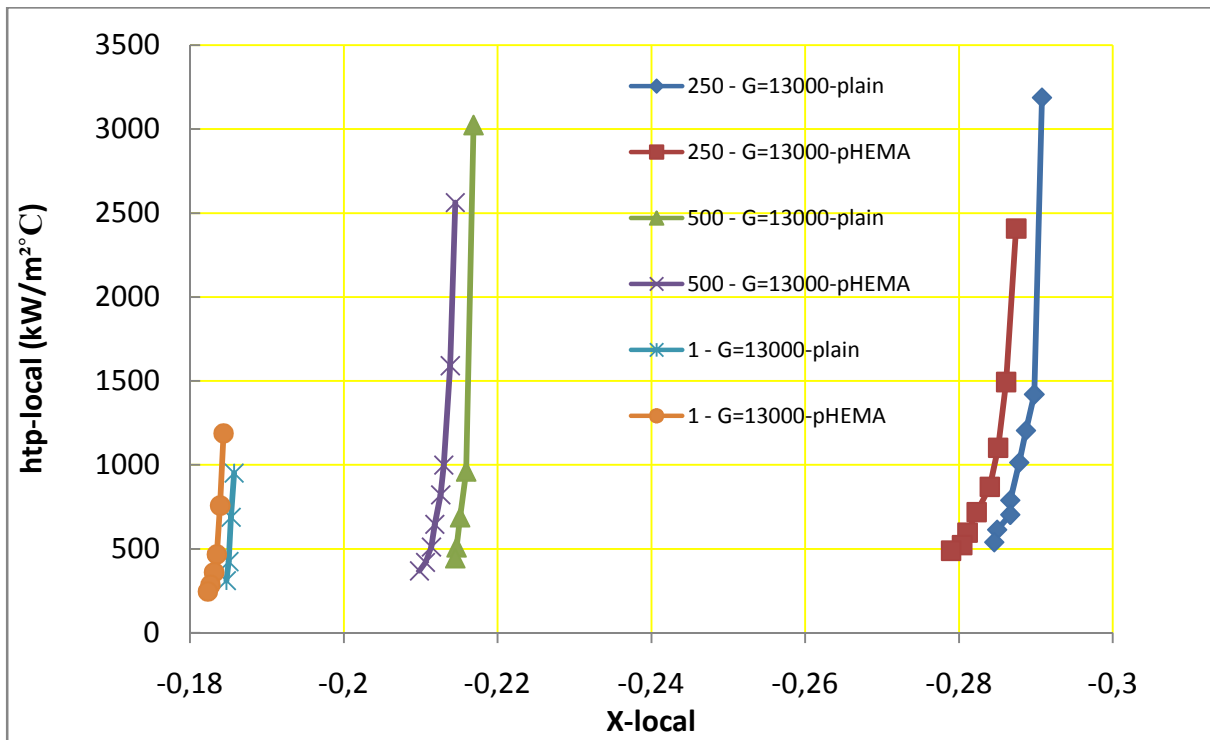
Figure 3-35: Heat transfer coefficient vs X_{local} for G = 13000 kg/m^{2}s

CHAPTER 4

CONTRIBUTION TO THE SCIENTIFIC KNOWLEDGE

The need for more efficient cooling solutions for microscale systems continuously increasing. Microchannel heat sinks and related flow boiling methods are efficient tools for overcoming this need. The experimental investigations performed in this thesis study is to contribute to the literature in two-phase flow boiling field. The first part, boiling instabilities in microchannels, contributes to scientific knowledge by:

- Proposing important data for understanding the physics behind the unstable boiling conditions
- Proving that FFT and side lobe energies obtained from the FFT analysis is a very useful tool and detection technique for predicting premature dryout in channels
- Showing that the flow restrictors at the microtube inlets have a significant effect on expanding boiling curves in microchannels.

The second part, ultra high mass flux flow boiling, contributes to scientific knowledge by:

- Proving that very high heat removal rates (>30000 kg/m^{2}s) can be achieved using ultra high mass flux conditions, which could be very useful for cooling of the applications that dissipates large amount of heat.
- Developing a new CHF correlation for the most accurate data fitting of the experimental data

The third part, high mass flux flow boiling on nanostructre coated microchannels, contributes to scientific knowledge by:

- Proving that pHEMA coating on microchanels can increase the heat transfer rate and enhance the CHF value, by forming an extra wetting layer on tube walls due to its swelling property in aquaeous medium.
- The iCVD is a useful tool for coating microchannels having various hydraulic diameters because of its 3D coating capability.

CHAPTER 5

CONCLUSIONS AND FUTURE WORK

In the first part, experimental tests were performed in micro tubes with ~254 μm and ~685 μm inner diameters at mass fluxes varying from G=78,9 - 276,3 kg/m^{2}s under boiling conditions prone to boiling instabilities. The effect of inlet restriction configurations, mass flux, and the effect of the microtube size on boiling instabilities were investigated. Temperature and pressure fluctuation peak to peak amplitudes and FFT profiles of the corresponding experiment parameters were illustrated for comparison. The major findings of this study are:

- Inlet restrictions have significant effect on expanding the CHF boiling curve, where an exponential rise in CHF values was observed with increasing restriction ratios.

- The introduction of the inlet restriction via valves yielded more stable boiling conditions by reducing the pressure and temperature fluctuation amplitudes, which is also more effective on higher restriction ratios.

- The micro tube size has a significant effect on the boiling instability phenomenon. At a given mass flux and heat flux value, the larger hydraulic diameters yield less effective results of expanding boiling curve.

- The promising FFT result profiles to be a very useful tool for the prediction of premature dryout in microchannels and reveals the merit for conducting further research.

In the second part, experimental tests were performed in microchannels having inner hydraulic diameters of ~ 250 μm, ~500 μm at ultra high mass flux values varying between 20511 kg/m^{2}s – 38111 kg/m^{2}s. The CHF values for corresponding mass fluxes were

comparatively investigated. The effect of heated length-inner diameter ratio (L_h/d_i) on CHF values was discussed. The obtained low exit mass quality (x_e <0,1) and the mentioned ultra high mass flux values show that mainly departure from nucleate boiling type CHF was observed during the experiments. During the experiments, heat transfer results that were never achieved (>30000 W/cm^2) via flow boiling were attained. The experimental results were compared to the existing CHF prediction correlations in the literature, and a new modified correlation for CHF prediction was established. The major findings of this study are:

- CHF increases linearly with mass flux unlike the weak trend that was mentioned in some of the previous studies in the related literature.
- L_h/d_i ratio has a significant meaning for CHF value, where the CHF decreases with increasing L_h/d_i ratio, similar to the other studies in the literature. The rate of decrease gets less as the ratio increases.
- The microtube hydraulic diameter has an inverse relation with CHF value, probably because of the more pronounced bubble-channel interaction at smaller scales since vapor constitutes a bigger space inside the smaller channels, thus the CHF effects gain importance.
- A new CHF prediction correlation was deduced based on the correlation of Sarma et al. [52], by using Curve Fitting using Least Square Method for the most accurate fitting to the other CHF data in the literature.

In the third part, tests were performed in pHEMA coated and plain microchannels having inner diameters of ~ 250 μm, ~500 μm and ~1 mm at two mass flux values, namely 10000 kg/m^{2}s and 13000 kg/m^{2}s. The CHF and T_{w-CHF} enhancement of pHEMA coating was comparatively investigated. The effects of microchannel hydraulic diameter on CHF were discussed according to the deduced results. The effect of mass flux on CHF was also investigated, whilst the mass flux values kept high in order to achieve subcooled boiling conditions and low exit qualities. The main findings of this study are:

- The swelling property of the coated pHEMA on microtubes has a significant effect on enhancing the CHF value and T_{w-CHF} in comparison to plain microtubes, due to the formed extra wetting layer that mitigates the insulation caused by vapor blanket.

- Coated pHEMA increases the heat removal rate by constituting an increased heat transfer area on the inner tube walls.
- CHF value is linearly dependant on the mass flux, which is more significant in smaller scales, since the liquid replenishment becomes important for delaying effects on the channel walls happening at CHF condition.
- The CHF has an inverse dependency to the channel hydraulic diameter, due to the more significant bubble-channel interaction where bubbles constitute a bigger space inside the channels.
- The iCVD was proven to be a very practical tool for coatings on microchannels with a wide range of hydraulic diameter, due to its 3D coating ability.

REFERENCES

[1] Siu-Ho, A. M., Qu, W., 2006, "Pressure drop and heat transfer in a sıngle-phase Micro-pin-fin heat sink", 2006 ASME International Mechanical Engineering Congress and Exposition (IMECE), November 5-10, Chicago, İllinois, USA

[2] Kandlikar, S. G., 2001, "Critical heat flux in subcooled flow boiling – An assessment of current understanding and future directions for research", Multiphase Science and Technology, 13 (3), pp. 207-232.

[3] Liu, D., Garimella, S. V., 2007, "Flow Boiling Heat Transfer in Microchannels", Journal of Heat Transfer, 129, pp. 1321-1332.

[4] Tong, W., Bergles, A. E., Jensen, M. K., 1998, "Pressure drop with highly subcooled flow boiling in small-diameter tubes", Experimental Thermal and Fluid Science, 15 (3), pp. 202-212.

[5] Federzoni, L., Revirand, P., 2008, "Micro-channelled heat exchanger manufactured by Ceramic Injection Moulding and co-firing", PIM International, 2 (3), pp. 69-71.

[6] Kuo, C. –J., Peles, Y., 2008, "Flow Boiling Instabilities in Microchannels and Means for Mitigation by Reentrant Cavities", Journal of Heat Transfer, 130, 072402-1-10

[7] Lee, Y. H., Chang, S. H., 2003, "The effect of vibration on critical heat flux in a vertical round tube", Journal of Nuclear Science and Technology, 40 (10), pp. 734-743.

[8] Cooke, D., Kandlikar, S.G., 2010," Pool boiling heat transfer and bubble dynamics over plain and enhanced microchannels", Proceedings of ASME 2010 3rd Joint US-European Fluids Engineering Summer Meeting and 8th International Conference on Nanochannels, Microchannels, and Minichannels, August 1-5, Montreal, Canada

[9] Lee, J., Mudawar, I., 2005, "Two-phase flow in high-heat-flux micro-channel heat sink for refrigeration cooling applications: Part I- pressure drop characteristics", International Journal of Heat and Mass Transfer, 48, pp. 928-940.

[10] Barber, J., Sefiane, K., Brutin, D., and Tadrist, L., 2010, "Hydrodynamics, heat transfer and flow boiling instabilities in microchannels", University of Edinburgh – Engineering and Electronics PhD Thesis Collection.

[11] Chang, M.H., Chen, F., and Fan, N-S., 2006, "Analysis of membraneless fuel cell using laminar flow in a Y-shaped microchannel", Journal of power sources, 159 (2), pp. 810-816.

[12] Tabeling, P., "Introduction to Microfluidics", Oxford University Press, Ch.1, 2005.

[13] Moriñigo, J.A., and Quesada J.H., 2010, "Solid–gas surface effect on the performance of a MEMS-class nozzle for micropropulsion ", Sensors and Actuators A:Physical, 162(1), pp. 61-71.

[14] Tsuyoshi, S., Makoto, T., Yoshiaki, N., Shintaro, N., Yusaku, K., Takayasu, S., and Takao, S., 2007, "A large-area wireless power-transmission sheet using printed organic transistors and plastic MEMS switches", Natural Materials, 6, pp. 413 – 417.

[15] Sinclair, M.J., 2000, "A high force low area MEMS thermal actuator", The7[th]Intersociety Conference on 2000.

[16] Rebello, K.J., 2004, "Applications of MEMS in surgery", Proceedings of the IEEE, 92(1), pp. 43- 55.

[17] Bertsch, Stefan S.; Groll, Eckhard A.; and Garimella, Suresh V., 2008, "Flow Boiling Heat Transfer in Microchannel Cold Plate Evaporators for Electronics Cooling", International Refrigeration and Air Conditioning Conference, Purdue, July 14-17, Paper 962.

[18] Garimella, S.V., Singhal, V., and Dong, L., 2006, "On-Chip Thermal Management With Microchannel Heat Sinks and Integrated Micropumps", Purdue University Purdue, 94(8), pp.1534 – 1548.

[19] Hassan, I., 2006, "Thermal-Fluid MEMS Devices: A Decade of Progress and Challenges Ahead", Journal of Heat Transfer, 128(11), pp. 1221 – 1234.

[20] Kosar, A., Ozdemir, M.R., and Keskinoz, M., 2010, "Pressure drop across micro-pin heat sinks under unstable boiling conditions", International Journal of Thermal Sciences, 49, pp. 1253-1263.

[21] Wang, G., and Cheng, P., 2008, "An experimental study of flow boiling instability in a single microchannel", International Communications in Heat and Mass Transfer, 35(10), pp. 1229-1234.

[22] Bogojevic, D., Sefiane, K., Walton, A.J., Lin, H., and Cummins, G., 2009, "Two-phase flow instabilities in a silicon microchannels heat sink", International Journal of Heat and Fluid Flow, 30(5), pp. 854-867.

[23] Bergles, A.E., Kandlikar, S.G., 2005, "On the Nature of Critical Heat Flux in Microchannels", Journal of Heat Transfer, 127, pp. 101.

[24] Yan, Y., Kenning, D.R.B., 1998, "Pressure fluctuations during boiling in a narrow channel", HTFS Research Symposium.

[25] Kenning, D.R.B., and Yan, Y., 2001, "Saturated flow boiling of water in a narrow channel, experimental investigation of local phenomena", Icheme Trans. A, Chem. Eng. Des. ,79, pp. 425–436.

[26] Brutin, D., Topin, F., and Tadrist, L., 2003, "Experimental study of the unsteady convective boiling in heated minichannels", Int. J. Heat Mass Transfer, 46, pp. 2957–2965.

[27] Kennedy, J.E, Dowling, G.M. Roach Jr., Abdel-Khalik, M.F., Ghiaassiaan, S.I., Jeter, S.M., and Quershi, S.M., 2000, "The onset of flow instability in uniformly heated horizontal micro-channels", J. Heat Transfer, 122, pp. 118–125.

[28] Kandlikar, S.G., Steinke, M.E., Tian, M.E., and Campbell, L.A., 2001, "High-speed photographic observation of flow boiling of water in parallel mini-channels, In: Proc. 2001, National Heat Transfer Conference, Anaheim, CA", 10–12 June.

[29] Kandlikar, S.G., 2002, "Fundamental issues related to flow boiling in minichannels and microchannels", Exp. Therm. Fluid Sci. 26 (2–4), pp. 389–407.

[30] Hetsroni, G., Klein, D., Mosyyak, A., Segal Z., and Pogrebnyak, E., 2003, "Convective boiling in parallel micro-channels". In: Kandlikar, Editor, First Int. Conf. Microchannels and Minichannels, April 24–25, Rochester, ASME, New-York, USA, pp. 59–67.

[31] Qu, W., and Mudawar, I., 2003, "Measurement and prediction of pressure drop in two-phase micro-channels heat sinks", Int. J. Heat Mass Transfer 46, pp. 2737–2753.

[32] Consolini, L., and Thome, J.R., 2009, "Microchannel convective heat transfer with flow instabilities", ECI International Conference on Boiling Heat Transfer, Florianópolis-SC-Brazil, 3-7 May.

[33] Zhang, T., Peles, Y., Wen, J.T., Tong, T., Chang, J-Y., Prasher, R., and Jensen, M.K., 2010, "Analysis and active control of pressure-drop flow instabilities in boiling microchannel system", International Journal of Heat and Mass Transfer, 53, pp. 2347-2360.

[34] Chen, T., and Garimella, S.V., 2011, "Local heat transfer distribution and effect of instabilities during flow boiling in a silicon microchannel heat sink," International Journal of Heat and Mass Transfer, 54, pp. 3179-3190.

[35] Bogojevic D., Sefiane K., Walton A.J., Lin H., Cummins G., Kenning D.B.R., and Karayiannis T.G., "Experimental investigation of non-uniform heating effect on flow boiling instabilities in a microchannel-based heat sink", International Journal of Thermal Sciences, 50, pp. 309 – 324.

[36] Kosar, A., Kuo, C. J., Peles, Y., 2006, "Suppression Of Boiling Flow Oscillations In Parallel Microchannels By Inlet Restrictors", J. Heat Transfer, 128, Issue 3, pp. 251-260.

[37] Wang, G., and Cheng, P., 2008, "An Experimental Study of Flow Boiling Instability in a Single Microchannel", International Communications in Heat and Mass Transfer, **35**, pp. 1229-1234.

[38] Bogojevic, D., Sefiane, K., Walton, A.J., Lin, H., and Cummins, G., 2009, "Two-phase Flow Instabilities in a Silicon Microchannels Heat Sink", International Journal of Heat and Fluid Flow, **30**, pp. 854-867.

[39] Lee, J., and Mudawar, I., 2009, "Critical Heat Flux for Subcooled Flow Boiling in Micro-channel Heat Sinks", International Journal of Heat and Mass Transfer, **52**, pp. 3341-3352.

[40] Mudawar, I., 2011, "Two-phase microchannel heat sinks: theory, applications and limitations", In: Proceedings of the ASME 2011 8th Thermal Engineering Conference, March, Honolulu, HI, AJTEC2011-44005.

[41] Kandlikar, S.G., Shoji, M., and Dhir, V.K., 1999, Handbook of Phase Change, *Taylor & Francis*, USA, Chapter 15, pp. 376.

[42] Wang, G., and Cheng, P., 2009, "Subcooled Flow Boiling and Microbubble Emission Boiling Phenomena in a Partially Heated Microchannel", International Journal of Heat and Mass Transfer, **52**, pp.79-91.

[43] Haynes, B.S., and Fletcher, D.F., 2003, "Subcooled Flow Boiling Heat Transfer in Narrow Passages", International Journal of Heat and Mass Transfer, **46**, pp. 3673-3682.

[44] Callizo, C.M., Palm, B., and Owhaib, W., 2007, "Subcooled Flow Boiling of R-134a in Vertical Channels of Small Diameter", International Journal of Multiphase Flow, **33**, pp. 822-832.

[45] Kosar A., 2011, "Flow Boiling in Microscale at High Flowrates", In: Proceedings of the ASME ICNMM 2011, February, Edmonton, Canada, ICNMM2011-58289.

[46] Ozdemir, M.R., Kaya, A., and Kosar, A., 2011, "Low Mass Quality Flow Boiling in Microtubes at High Mass Fluxes", ASME Journal of Thermal Sciences and Engineering Applications, **3**(4), 041001 (9 pages).

[47] Kandlikar, S.G., 2001," A theoretical model to predict pool boiling CHF incorporating effects of contact angle and orientation", Journal of Heat Transfer, 123, pp. 1071-1079.

[48] Koşar, A., Peles, Y., Bergles, A.E., 2009, "Experimental investigation of critical heat flux in microchannels for flow-field probes", ASME 2009 7th ICNMM, June 22-24, Pohang, South Korea.

[49] Lee, P.S., and Garimella, S.V., 2008, "Saturated Flow Boiling Heat Transfer and Pressure Drop in Silicon Microchannel Arrays", International Journal of Heat and Mass Transfer, **51**, pp. 789-806.

[50] Collier, J.G., and Thome, J.R., 2001, Convective Boiling and Condensation, *Oxford Science Publications*, UK, Chapter 5, pp. 203.

[51] Ghiaasiaan, S.M., 2008, Two Phase Flow Boiling and Condensation in Conventional and Miniature System, *Cambridge University Press*, UK, Part II, pp. 348.

[52] Sarma, P.K., Srinivas, V., Sharma, K.V., Dharma Rao, V. and Celata, G.P., 2006, A correlation to evaluate critical heat flux in small diameter tubes under subcooled conditions of the coolant, Int. J. Heat Mass Transfer, 49, 42-51.

[52] Khlebtsov, G.N. and Dykman, L.A., 2010, "Optical Properties and Biomedical Applications of Plasmonic Nanoparticles", Journal of Quantitative Spectroscopy and Radiative Transfer, **111**(1), pp. 1-35.

[53] Baffou, G., Quidant, R., and Abajo, F.J.G., 2010, "Nanoscale Control of Optical Heating in Complex Plasmonic Systems", ACSNANO, **4**(2), pp. 709-716.

[54] DiMatteo, R.S., Greiff, P., Finberg, S.L., Young-Waithe, K., Choy, H.K.H., Masaki, M.M., and Fonstad, C.G., 2001, "Enhanced Photogeneration of Carriers in a Semiconductor via Coupling across a Nonisothermal Nanoscale Vacuum Gap," Appl. Phys. Lett., **79**, pp. 1894.

[55] Fu, C.J., and Zhang, Z.M., 2006, "Nanoscale Radiation Heat Transfer for Silicon at Different Doping Levels," International Journal of Heat and Mass Transfer, **49**(9-10), pp. 1703-1718.

[56] Fu, C.J. and Tan, W.C., 2009, "Near-Field Radiative Heat Transfer between Two Plane Surfaces with One Having a Dielectric Coating," Journal of Quantitative Spectroscopy and Radiative Transfer, 110 (12), pp. 1027-1036.

[57] Sendur, K., Peng, C., and Challener, W., 2005, "Near Field Radiation from a Ridge Waveguide Transducer in the Vicinity of a Solid Immersion Lens," Phys. Rev. Lett., **94**(4), pp. 043901.

[58] Rousseau, E., Siria, A., Jourdan, G.,Volz, S., Comin, F., Chevrier, J. and Greffet, J.-J., 2009, "Radiative Heat Transfer at the Nanoscale," Nature Photon., **3**, pp. 514-517.

[59] Sendur, K., and Baran, E., 2009, "Near-field power transmission of dipole nano-antennas", Applied Physics B, **96**, pp. 325-335.

[60] Şendur, K., Koşar, A., Mengüç, M. P., 2011, "Localized radiative energy transfer from a plasmonic bow-tie nano-antenna to a magnetic thin film stack", Applied Physics A – Materials Science & Processing, 103 (3), pp. 703-707.

[61] Kandlikar, S.G., Shoji, M., and Dhir, V.K., Handbook of Phase Change, *Taylor & Francis*, USA, Chapter 15, pp. 443, 1999.

[62] Khanikar, V., Mudawar, I., Fisher, T., 2009, "Effects of carbon nanotube coating on flow boiling in a microchannel", International Journal of Heat and Mass Transfer, 52, pp. 3805-3817.

[63] Sarwar, M.S., Jeong, Y. H., Soon, H. C., 2007, "Subcooled flow boiling CHF enhancements with porous surface coatings", International Journal of Heat and Mass Transfer, 50, pp. 3649-3657.

[64] Phan, H.T., Caney, N., Marty, P., Colasson, S., Gavillet, J., 2012, "Flow Boiling of Water on Nanocoated Surfaces in a Microchannel, J. Heat Transfer 134, 020901

[65] Morshed, A.K.M.M., Fanghao Yang, M. Yakut Ali, Khan, J.A., Li, C., 2012, "Enhanced flow boiling in a microchannel with integration of nanowires", Applied Thermal Engineering, 32, pp. 68-75.

[66] Ahn, S.H., Lee, C., Kim., H., Jo, H., Kang, S., Kim, J., Shin, J., Kim, M.H., 2010, "Pool Boiling CHF Enhancement By Micro/Nanoscale Modification Of Zircaloy-4 Surface", Nuclear Engineering and Design, 240 (10), pp. 3350-3360.

[67] Ahn, H.S., Kim, M.H., 2011, "The effect of micro/nanoscale structures on CHF enhancement", Nuclear Engineering and Technology, 43, pp. 205-216.

[68] Ahn, H.S., Kang, S. H, Lee, C., Kim., J., Kim, M. H., 2012, "The effect of liquid spreading due to micro-structures of flow boiling critical heat flux", International Journal of Multiphase Flow, 43, pp. 1-12.

[69] Kandlikar, S.G., Shoji, M., and Dhir, V.K., Handbook of Phase Change, *Taylor & Francis*, USA, Chapter 15, pp. 444, 1999.

[70] Celata, G. P., Cumo, M., Mariani, A., Simoncini, M., and Zummo, G., 1994c, "Rationalization of existing mechanistic models for the prediction of water subcooled flow boiling critical heat flux", International Journal of Heat and Mass Transfer, 37 (7 Suppl. 1), pp 347-360.

[71] Kandlikar, S.G., Shoji, M., and Dhir, V.K., Handbook of Phase Change, *Taylor & Francis*, USA, Chapter 15, pp. 457, 1999.

[72] U.S. Department of Energy Fundamentals Handbook, "Thermodynamics, Heat Transfer and Fluid Flow", Distribution, 1992, 2, pp. 43.

[73] Omidian, H., Park, K., Kandalam, U., Rocca, J. G., 2010, "Swelling and Mechanical Properties of Modified HEMA-based Superporous Hydrogels", Journal of Bioactive and Compatible Polymers, 25, pp. 485-497.

[74] MacBain, S. M., and Bergles, A. E., 1995, "Heat Transfer and Pressure Drop Characteristics of a Forced Convective Evaporation in Deep Spirally Fluted Tubing", Proceedings of Convective Flow Boiling, Banff, Alberta, Canada, April 30- May 5.

[75] Huh, C., Kim, J., Kim, M. H., 2007, "Flow pattern transition instability during flow boiling in a single microchannel", International Journal of Heat and Mass Transfer, 50, pp. 1049-1060.

[76] Wu, H. Y., Cheng, P., 2002, "Visualization and Measurements of Periodic Boiling in Silicon Microchannels", International Journal of Heat and Mass Transfer, 46, 2603-2614.

[77] Brutin. D., Tadrist, L., 2004, "Pressure Drop and Heat Transfer Analysis of Flow Boiling in a Minichannel: Influence of the Inlet Condition on Two-Phase Flow Stability", International Journal of Heat and Mass Transfer, 47, pp. 2365-2377.

[78] A.V. Oppenheim, R.W. Schafer, Discrete-time Signal Processing, second ed. Prentice Hall Signal Processing Series, 1999.

[79] Bergles, A, E., 1963, "Subcooled burnout in tubes of small diameter", ASME Paper No. 63-WA-182.

[80] Celata, G. P., 1993, "Recent achievements in the thermal hydraulics of high heat flux components in fusion reactors", Experimental Thermal and Fluid Science, 7(4), pp. 263-278.

[81] Vandervort, C. L., Bergles, A. E., Jensen, M. K., 1994, "An experimental study of critical heat flux in very high heat flux subcooled boiling", International Journal of Heat and Mass Transfer, 37 (1), pp. 161-173.

[82] Hall, D. D., Mudawar, I., 2000, "Critical heat flux (CHF) for water flow in tubes – II: Subcooled CHF correlations", International Journal of Heat and Mass Transfer, 43 (14), pp. 2605-2640.

[83] Koşar, A., Peles, Y., Bergles, A.E., 2009, "Experimental investigation of critical heat flux in microchannels for flow-field probes", ASME 2009 7th ICNMM, June 22-24, Pohang, South Korea.

[84] Liu, M-Y., Tang, X-P., and Jiang, F., 2004, "Studies on the hydrodynamic and heat transfer in a vapor-liquid-solid flow boiling system with a CCD measuring technique", Chemical Engineering Science, 59(4), pp. 889-899.

[85] Kandlikar, S.G., Shoji, M., and Dhir, V.K., Handbook of Phase Change, *Taylor & Francis*, USA, Chapter 15, pp. 368, 1999.

[86] Trujillo, N.J., Baxamusa, S.H., Gleason, K. K., 2009, "Grafted Functional Polymer Nanostructures Patterned Bottom-Up by Colloidal Lithography and Initiated Chemical Vapor Deposition (iCVD)", Chem. Mater. 2009, 21, pp 742-750.

[87] Chan, K., Gleason, K.K., 2005, "Initiated chemical vapor deposition of linear and cross-linked poly (2-hydroxyethyl methacrylate) for use as thin-film hydrogels", Langmuir, 21 (19), pp. 8930-8939.

[88] Koşar, A., 2009, "A model to predict saturated critical heat flux in minichannels and microchannels", International Journal of Thermal Sciences, 48 (2), pp. 261-270.

[89] Lau, K. K., Gleason, K. K., 2006, "Initiated chemical vapor deposition (iCVD) of poly (alkyl acrylates): A kinetic model", Macromolecules, 39 (10), pp. 3695-3703.